



Barium and carbon fluxes in the Canadian Arctic Archipelago

Helmuth Thomas, Elizabeth Shadwick, Frank Dehairs, Bruno Lansard, Alfonso Mucci, Jacques Navez, Yves Gratton, Friederike Prowe, Melissa Chierici, Agneta Fransson, et al.

► To cite this version:

Helmuth Thomas, Elizabeth Shadwick, Frank Dehairs, Bruno Lansard, Alfonso Mucci, et al.. Barium and carbon fluxes in the Canadian Arctic Archipelago. *Journal of Geophysical Research*, 2011, 116, pp.C00G08. 10.1029/2011JC007120 . hal-00662988

HAL Id: hal-00662988

<https://hal.science/hal-00662988>

Submitted on 25 Jan 2012

HAL is a multi-disciplinary open access archive for the deposit and dissemination of scientific research documents, whether they are published or not. The documents may come from teaching and research institutions in France or abroad, or from public or private research centers.

L'archive ouverte pluridisciplinaire **HAL**, est destinée au dépôt et à la diffusion de documents scientifiques de niveau recherche, publiés ou non, émanant des établissements d'enseignement et de recherche français ou étrangers, des laboratoires publics ou privés.

1 Barium and carbon fluxes in the Canadian Arctic Archipelago

2 Helmuth Thomas,¹ Elizabeth Shadwick,^{1,2} Frank Dehairs,³ Bruno Lansard,⁴
 3 Alfonso Mucci,⁴ Jacques Navez,³ Yves Gratton,⁵ Friederike Prowe,⁶ Melissa Chierici,⁷
 4 Agneta Fransson,⁸ Tim N. Papakyriakou,⁹ Erika Sternberg,¹ Lisa A. Miller,¹⁰
 5 Jean-Éric Tremblay,¹¹ and Christophe Monnin¹²

6 Received 9 March 2011; revised 3 August 2011; accepted 8 September 2011; published XX Month 2011.

7 [1] The seasonal and spatial variability of dissolved Barium (Ba) in the Amundsen Gulf,
 8 southeastern Beaufort Sea, was monitored over a full year from September 2007 to
 9 September 2008. Dissolved Ba displays a nutrient-type behavior: the maximum water
 10 column concentration is located below the surface layer. The highest Ba concentrations
 11 are typically observed at river mouths, the lowest concentrations are found in water
 12 masses of Atlantic origin. Barium concentrations decrease eastward through the Canadian
 13 Arctic Archipelago. Barite (BaSO₄) saturation is reached at the maximum dissolved
 14 Ba concentrations in the subsurface layer, whereas the rest of the water column is
 15 undersaturated. A three end-member mixing model comprising freshwater from sea-ice
 16 melt and rivers, as well as upper halocline water, is used to establish their relative
 17 contributions to the Ba concentrations in the upper water column of the Amundsen
 18 Gulf. Based on water column and riverine Ba contributions, we assess the depletion of
 19 dissolved Ba by formation and sinking of biologically bound Ba (bio-Ba), from which
 20 we derive an estimate of the carbon export production. In the upper 50 m of the water
 21 column of the Amundsen Gulf, riverine Ba accounts for up to 15% of the available
 22 dissolved Ba inventory, of which up to 20% is depleted by bio-Ba formation and export.
 23 Since riverine inputs and Ba export occur concurrently, the seasonal variability of
 24 dissolved Ba in the upper water column is moderate. Assuming a fixed organic carbon to
 25 bio-Ba flux ratio, carbon export out of the surface layer is estimated at $1.8 \pm 0.45 \text{ mol C}$
 26 $\text{m}^{-2} \text{yr}^{-1}$. Finally, we propose a climatological carbon budget for the Amundsen Gulf
 27 based on recent literature data and our findings, the latter bridging the surface and
 28 subsurface water carbon cycles.

29 **Citation:** Thomas, H., et al. (2011), Barium and carbon fluxes in the Canadian Arctic Archipelago, *J. Geophys. Res.*, 116,
 30 XXXXXX, doi:10.1029/2011JC007120.

¹Department of Oceanography, Dalhousie University, Halifax, Nova Scotia, Canada.

²Now at Antarctic Climate and Ecosystems Cooperative Research Center, Hobart, Tasmania, Australia.

³Earth System Sciences and Analytical and Environmental Chemistry, Vrije Universiteit Brussel, Brussels, Belgium.

⁴Department of Earth and Planetary Sciences, McGill University, Montreal, Quebec, Canada.

⁵INRS-ETE, Quebec, Quebec, Canada.

⁶Leibniz Institute of Marine Sciences at University of Kiel (IFM-GEOMAR), Kiel, Germany.

⁷Department of Chemistry, University of Gothenburg, Göteborg, Sweden.

⁸Department of Earth Sciences, University of Gothenburg, Göteborg, Sweden.

⁹Center for Earth Observation Science, University of Manitoba, Winnipeg, Manitoba, Canada.

¹⁰Institute of Ocean Sciences, Fisheries and Oceans Canada, Sidney, British Columbia, Canada.

¹¹Department de Biologie, Université Laval, Quebec, Quebec, Canada.

¹²Laboratoire Mécanismes et Transferts en Géologie, CNRS-Université Paul Sabatier, Toulouse, France.

1. Introduction

[2] Barium (Ba) has increasingly been employed as water mass tracer and as biogeochemical proxy of biological productivity. Here, we combine both approaches in order to gain insights into the biogeochemistry of Ba and its relationship to the inorganic carbon cycle in the Canadian Arctic Archipelago. Finally, we use dissolved Ba data to assess export production of organic carbon, which in turn enables us to balance the carbon budget for our investigation area. [3] The strong correlation between the distributions of barium bound to particulate organic matter (bio-Ba) and particulate organic carbon (C_{org}) in the oceans and sediments has led to the use of bio-Ba as a proxy of biological productivity, in particular of export production from seasonal to geological time scales [e.g., Bishop, 1988; Dehairs et al., 1992, 1997; Dymond et al., 1992; Francois et al., 1995; Dymond and Collier, 1996; Gillikin et al., 2006; Sternberg et al., 2007; Calvert and Pederson, 2007]. As summarized by Sternberg et al. [2007], aggregates containing bio-Ba are formed in the upper water column. Accordingly, the highest

51 bio-Ba concentrations are typically observed in surface
 52 waters, although such maxima may be less accentuated or
 53 missing in certain regions or seasons. A subsurface maximum
 54 of bio-Ba is also often observed in the mesopelagic layer and
 55 primarily consists of barite (BaSO_4) micro-crystals [Bishop,
 56 1988; Dehairs et al., 1997; Jeandel et al., 2000; Jacquet
 57 et al., 2007; Sternberg et al., 2008; Dehairs et al., 2008].
 58 The presence of barite micro-crystals in oceanic suspended
 59 particulate matter is quite ubiquitous, despite the fact that most
 60 ocean waters are undersaturated with respect to this mineral
 61 [Monnin et al., 1999]. Several hypotheses have been proposed
 62 to explain this conundrum [e.g., Bishop, 1988; Dehairs et al.,
 63 1997; Sternberg et al., 2005, 2008; van Beek et al., 2009],
 64 most of which call upon biological processes including
 65 respiratory activity in the mesopelagic layer [Dehairs et al.,
 66 1992]. A detailed review of these hypotheses is discussed
 67 by Sternberg et al. [2007], and Jacquet et al. [2011] sum-
 68 marize these by reporting that barite precipitates in super-
 69 saturated microenvironments during the bacterial degradation
 70 of sinking organic matter. In other words, organic particles
 71 that escape breakdown during settling through the water col-
 72 umn accumulate barite, thus explaining the observed depth-
 73 dependent increase of Ba fluxes [e.g., Francois et al., 1995].
 74 [4] The continual formation of barite in biogenic aggre-
 75 gates, which settle through the water column, serves to increase
 76 Ba fluxes with depth and thus lowers the organic carbon to
 77 bio-Ba ($C_{\text{org}}:\text{bio-Ba}$) flux ratio with depth. Moreover, this
 78 ratio decreases with depth as a result of the (preferential)
 79 respiration of organic carbon relative to the release or dis-
 80 solution of bio-Ba. Such observations have been reported in
 81 several, but not all regions of the deep oceans [Dymond et al.,
 82 1992, Francois et al., 1995], and thus the $C_{\text{org}}:\text{bio-Ba}$ flux
 83 ratios recorded in ocean basins vary regionally [Dymond
 84 et al., 1992; Francois et al., 1995; Dymond and Collier,
 85 1996]. On the other hand, Dymond et al. [1992] and
 86 Francois et al. [1995] have shown that within the euphotic
 87 zone and irrespective of the ocean basin, the $C_{\text{org}}:\text{bio-Ba}$ flux
 88 ratio converges to a value of approximately $C_{\text{org}}:\text{bio-Ba} =$
 89 $200 \text{ g C (g Ba)}^{-1}$ [$2290 \text{ mol C (mol Ba)}^{-1}$], close to
 90 the globally estimated ratio $C_{\text{org}}:\text{bio-Ba} = 260 \text{ g C (g Ba)}^{-1}$
 91 [$2860 \text{ mol C (mol Ba)}^{-1}$] reported by Broecker and Peng
 92 [1982]. Higher $C_{\text{org}}:\text{bio-Ba}$ flux ratios have been observed
 93 in continental margins [Dehairs et al., 2000] and have been
 94 attributed to the formation of aggregates of both open ocean
 95 and margin carbon, and to differences in functioning of
 96 open ocean and marine ecosystems. Later in this paper,
 97 we exploit this fact to assess the export of marine carbon out
 98 of the euphotic zone, rather than an overall carbon export
 99 comprising terrestrial and marine carbon.

100 [5] It is difficult to quantitatively relate the behavior of
 101 particulate and dissolved Ba in the water column to each
 102 other, since, like Ca, dissolved Ba concentrations are 2–3
 103 orders of magnitude larger than those of particulate Ba [e.g.,
 104 Jacquet et al., 2005, 2007]. Dissolved Ba displays a nutrient-
 105 type profile, which is, as we later argue, primarily shaped by
 106 the generation of bio-Ba in the surface layer and the subse-
 107 quent release of Ba during the respiratory breakdown of the
 108 organic matter below the euphotic zone. In the mesopelagic
 109 and deep oceans, the formation and dissolution rates of barite
 110 (BaSO_4) also influence the vertical distributions and con-
 111 centrations of dissolved Ba. Dissolved Ba has been
 112 employed as a water mass tracer in various ocean basins,

including the Southern Ocean [e.g., Jacquet et al., 2005, 113
 2007; Hoppema et al., 2010], and has been most useful in 114
 the Arctic Ocean, since Arctic rivers draining the North 115
 American continent carry significantly higher dissolved Ba 116
 concentrations than their Eurasian counterparts [e.g., Cooper 117
 et al., 2008]. Few studies discuss factors that control the 118
 distribution of dissolved Ba in the water column of the Arctic 119
 region [e.g., Falkner et al., 1994; Guay and Falkner, 1997; 120
 Taylor et al., 2003; Guay et al., 2009]. Complemented by 121
 additional tracers, such as total alkalinity (A_T) or the stable 122
 oxygen isotope composition of seawater ($\delta^{18}\text{O}$), dissolved 123
 Ba has been used to determine the nature/origin and contri- 124
 bution of freshwater (sea-ice melt and river runoff) to Arctic 125
 Ocean surface waters [e.g., Falkner et al., 1994; Guay and 126
 Falkner, 1997, 1998; Cooper et al., 2008; Bates et al., 127
 2009; Yamamoto-Kawai et al., 2010]. In the surface 128
 waters, the concentrations of dissolved Ba reveal a high 129
 spatial variability with significantly enhanced concentrations 130
 of dissolved Ba close to the river mouths [e.g., Guay et al., 131
 2009; Yamamoto-Kawai et al., 2010]. Likewise, the strong 132
 seasonality of river runoff is reflected in the temporal vari- 133
 ability of the surface dissolved Ba concentrations in near- 134
 shore regions, a feature that has not been readily captured 135
 in recent studies because of the paucity of data during 136
 ice-covered seasons. In an attempt to circumvent this short- 137
 coming, Cooper et al. [2008] introduced the use of flow- 138
 weighted values of tracer concentrations, such as Ba in Arctic 139
 rivers. 140

[6] In the present work, we move beyond previous studies 141
 by documenting the spatial and temporal variability of dis- 142
 solved Ba in waters of the Canadian Arctic Archipelago 143
 over a complete annual cycle, as well as the relationship 144
 between Ba and measurable parameters of the inorganic 145
 carbon system, specifically the dissolved inorganic carbon 146
 (DIC) and A_T . We use results of a multitracer water mass 147
 analysis to assess the temporal evolution of freshwater 148
 addition and removal to/from the surface waters over the 149
 annual cycle, and compute the surface layer dissolved Ba 150
 deficiency - the difference between observed and “ideal” or 151
 conservative Ba concentrations - as a measure of bio-Ba 152
 formation. From this deficiency, we estimate the annual 153
 export of organic carbon (C_{org}) out of the euphotic zone and 154
 discuss the role of export and decay of bio-Ba below the 155
 surface layer in relation to the saturation state of waters with 156
 respect to barite. 157

2. Methods 158

2.1. Investigation Area 159

[7] This study was conducted in the framework of the 160
 International Polar Year on board the Canadian icebreaker 161
 CCGS Amundsen between September 2007 and September 162
 2008. Sampling in the Canadian Arctic Archipelago (CAA) 163
 took place at the beginning and end of the 12-month cruise 164
 at stations along an east-west section from Baffin Bay into 165
 the Eastern Beaufort Sea (Figure 1). The Amundsen Gulf, in 166
 the eastern Beaufort Sea (Figure 1), was sampled through 167
 a full annual cycle, for the ver’y first time, at approximately 168
 bi-weekly intervals, at somewhat higher frequency during 169
 spring and summer than during winter, when, by design, the 170
 ship was frozen into free-drifting floes for varying periods 171
 of time. For the subsequent annual analysis, we constructed 172

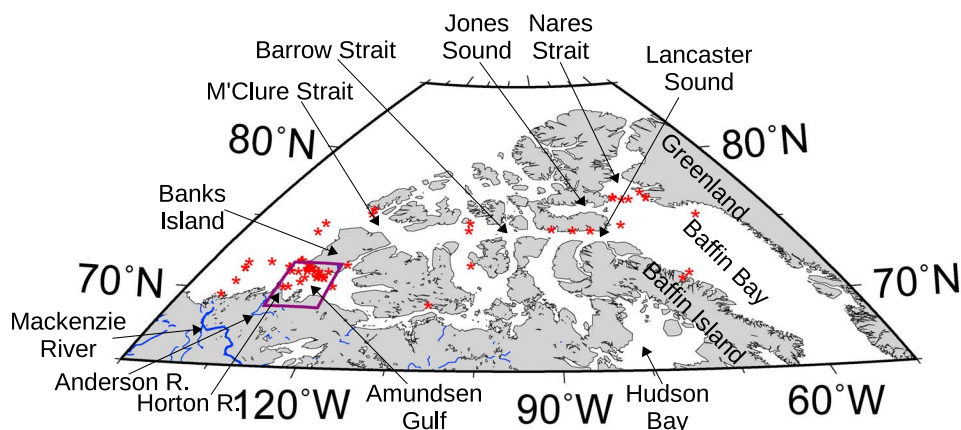


Figure 1. Investigation area. The stations sampled for dissolved Ba are indicated by red stars. The box encompasses the area 70°N–72°N, 121.8°W–126°W. The annual cycles and budgets reported in this paper were constructed from data collected at stations within this area. Hydrographic and carbonate system parameters are from higher temporal and spatial sampling densities [see *Shadwick et al.*, 2011b].

173 an annual cycle of observational data acquired in an area
174 defined by the boundaries: 70°N–72°N, 121.8°W–126°W
175 (Figure 1). Obviously, any considerations of interannual
176 variability would exceed the limitations of our data set.

177 2.2. Analytical Methods

178 [8] As part of the overall sampling program in the
179 Amundsen Gulf [e.g., *Shadwick et al.*, 2011b], we collected
180 seawater samples using a rosette system equipped with
181 24 12-L Niskin bottles at approximately 70 stations (includ-
182 ing repeats at different times of the year). Vertical profiles
183 of dissolved Ba concentrations were constructed from 8 to
184 12 depths per cast. Unfiltered seawater was transferred directly
185 from the spigot of the Niskin bottles into 30 mL plastic bottles,
186 acidified with 15 μL of concentrated Suprapur hydrochloric
187 acid and analyzed in the home laboratory using Isotope
188 Dilution Sector Field Inductively Coupled Plasma Mass
189 Spectrometry (SF-ICP-MS, Element 2, Thermo Finnigan).
190 Briefly, 1 g of seawater was spiked with 0.7 g of a ^{135}Ba -spike
191 solution yielding a $^{138}\text{Ba}/^{135}\text{Ba}$ ratio between 0.7 and 1 to
192 minimize error propagation. Subsequently the sample was
193 diluted with Milli-Q grade water to a final weight of 30 g.
194 Blanks consisted of acidified (with nitric acid) Milli-Q water.
195 Quantities of sample, spike and dilution water were accu-
196 rately assessed by weighing. Reproducibility of our method
197 is $\pm 1.5\%$ (RSD) as tested on repeat preparations of ref-
198 erence solutions. Average Ba values obtained for reference
199 waters SLRS-3 and an in-house standard (OMP, a Medi-
200 terranean Sea standard prepared by C. Jeandel) were $13.48 \pm$
201 $0.21 \mu\text{g l}^{-1}$ (1σ) with a RSD of 1.55% and $10.49 \pm 0.29 \mu\text{g}$
202 l^{-1} (1σ) with RSD of 2.75%, respectively, in good agreement
203 with certified values (SLRS-3: $13.4 \pm 0.6 \mu\text{g l}^{-1}$ and OMP:
204 $10.4 \pm 0.2 \mu\text{g l}^{-1}$). Overall precision (including sampling
205 precision) based on 6 dissolved Ba profiles sampled in a
206 hydrographically stable environment is $\pm 0.3 \mu\text{g l}^{-1}$ (1σ) with a
207 RSD of 5%. Please refer to *Dehairs et al.* [2008] and *Jacquet*
208 [2007] for further details. The Ba sampling was paralleled
209 by sampling for the stable isotope composition of seawater
210 ($\delta^{18}\text{O}$), of which samples were stored in 13 mL screw-
211 cap plastic test tubes without headspace. The $\delta^{18}\text{O}$ samples

were analyzed at the Geological Survey of Canada Delta- 212
Laboratory in Quebec City. Water samples were acidified 213
to pH ranging from 6 to 7 with orthophosphoric acid and 214
transferred without headspace to 4-mL vials containing 215
100 mg of copper to scavenge sulfide species and a few 216
grains of activated charcoal to scavenge organic volatiles. 217
After resting in the refrigerator for 5 days, 600 μL of water 218
were transferred to a 10-mL vial on a Gas Bench II and 219
equilibrated at 25°C for 5–7 days with a 0.5% CO_2 in 220
nitrogen gas mixture. The CO_2 gas was introduced and 221
analyzed in a Delta Plus mass ratio spectrometer. The oxygen 222
isotope ratio is expressed on the $\delta^{18}\text{O}$ notation, defined as the 223
 $^{18}\text{O}/^{16}\text{O}$ ratio of a sample relative to the Vienna Standard 224
Mean Ocean Water (V-SMOW) according to: 225

$$\delta^{18}\text{O} = \left(\left(^{18}\text{O}/^{16}\text{O} \right)_{\text{sample}} / \left(^{18}\text{O}/^{16}\text{O} \right)_{\text{V-SMOW}} - 1 \right) \times 10^3 [\text{‰}]$$

(1)

[9] The oxygen isotope composition of seawater was 226
measured to a precision of $\pm 0.05\text{‰}$, based on the analysis of 227
random duplicate samples. DIC and A_T were sampled 228
according to standard protocols [*Dickson et al.*, 2007] at 229
much higher spatial and temporal resolution, yielding more 230
than 2000 measurements. All samples were analyzed on 231
board by coulometric (DIC) and potentiometric (A_T) titration 232
using a VINDTA 3C (Versatile Instrument for the Deter- 233
mination of Titration Alkalinity, by Marianda, Germany). 234
Alternatively, A_T was also measured onboard using an 235
automated Radiometer® (Titrilab 865) potentiometric titra- 236
tor operated in continuous titrant addition mode. Routine 237
calibrations and analyses of Certified Reference Materials 238
(provided by A. G. Dickson, Scripps Institution of Ocean- 239
ography) ensured that the uncertainty of the DIC and A_T 240
measurements was less than 0.5%. Details of the sampling 241
and analytical methods, as well as in-depth scientific eval- 242
uations of the DIC and A_T data, have been provided by 243
Shadwick et al. [2011a, 2011b] and *Mucci et al.* [2010]. 244

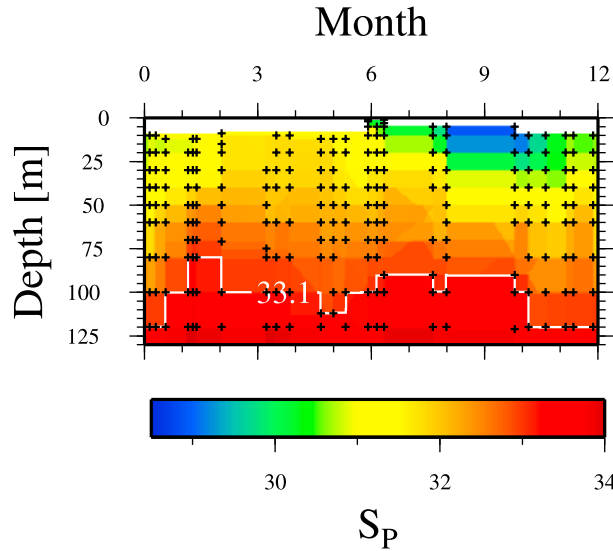


Figure 2. Temporal evolution of salinity in the surface waters of the Amundsen Gulf. Details of the seasonality of salinity and related carbon parameters have been discussed in detail by *Shadwick et al.* [2011b]. We have indicated the evolution of the $S_p = 33.1$ isopleth, which represents the lower boundary of our analysis.

2.3. Water Mass Decomposition

[10] As outlined in the following section, one of the objectives of this study was to establish a surface layer budget of dissolved Ba. Deviations from a conservative behavior of dissolved Ba were estimated and attributed to the formation of bio-Ba. Together with literature values for the $C_{org}:bio$ -Ba ratio in particulate organic matter, we estimate the export production out of the surface mixed layer (SML). The maximum surface mixed layer depth in the Amundsen Gulf is approximately 50 m, as determined from the position of the pycnocline (Figure 2) [see also *Chierici et al.*, 2011, Figure 2c; *Shadwick et al.*, 2011b]. We furthermore assess the dissolved Ba surplus concentrations in waters between 50 m depth and the level corresponding to the practical salinity (S_p) = 33.1 isopleth, in order to evaluate whether decay of bio-Ba occurs within this depth interval, just below the euphotic zone.

[11] In order to establish a dissolved Ba budget, we performed a regional water mass analysis in the upper water column, with the Upper Halocline Layer (UHL), characterized by $S_p = 33.1$ (Figure 2), as the deepest layer. In the Amundsen Gulf, the UHL water resides at a depth of 80–120 m (Figure 2). Our analysis thus encompasses the depth range of interest (0–50 m), as well as the layer between 50 m and $S_p = 33.1$ isopleth, located at approximately 100 m water depth for most of the year.

[12] The application of salinity (S) and A_T to distinguish the two major sources of freshwater, river runoff and sea-ice melt, to seawater is well established [e.g., *Yamamoto-Kawai and Tanaka*, 2005]. Here, we employ a three end-member mixing model to decompose the water masses of the surface layer in fractions of upper halocline water (F_{UHL}), meteoric water (F_{MW} ; river runoff + precipitation), and sea-ice melt (F_{SIM}). If the chemical properties of each end-member are

distinct and well defined, the relative contributions of these three water masses to a parcel of seawater can be computed from the following equations:

$$F_{MW} + F_{SIM} + F_{UHL} = 1 \quad (2)$$

$$F_{MW}S_{MW} + F_{SIM}S_{SIM} + F_{UHL}S_{UHL} = S \quad (3)$$

$$F_{MW}A_T(MW) + F_{SIM}A_T(SIM) + F_{UHL}A_T(UHL) = A_T \quad (4a)$$

$$F_{MW}\delta^{18}O_{(MW)} + F_{SIM}\delta^{18}O_{(SIM)} + F_{UHL}\delta^{18}O_{(UHL)} = \delta^{18}O \quad (4b)$$

[13] The decomposition was performed using two sets of equations: (2), (3), and (4a), as well as (2), (3), and (4b), meaning that we used either A_T or $\delta^{18}O$ together with salinity as tracers. In such analyses, as discussed for example by B. Lansard et al. (Seasonal variability of water mass distribution in the southeastern Beaufort Sea determined by total alkalinity and $\delta^{18}O$, submitted to *Journal of Geophysical Research*, 2011), each tracer has its individual strengths and weaknesses. For our purposes, relying on A_T tends to more accurately describe the contributions of sea-ice melt, at the expense of a slight underestimation of the river runoff. On the other hand, the use of $\delta^{18}O$, better describes the river runoff fraction, but tends to underestimate the sea-ice fraction. Since we gathered much more high quality A_T data than $\delta^{18}O$ data, we used salinity together with A_T for the water mass decomposition analysis. Consequently, our estimate of riverine Ba input should be considered as a conservative, lower bound.

[14] The end-member characteristics are given in Table 1. For the decomposition analysis, we assumed that S , A_T and the Ba concentration in sea-ice are null, i.e., on an annual cycle sea-ice does not constitute a net source or sink of these species to the underlying seawater. Rather these species are trapped during the ice formation in autumn and winter and are released again during ice melt. Considering the sea-ice concentrations of S , A_T , and Ba as being different from zero at annual or greater time scales, leads to an erroneous definition of ice as a source of these compounds, since the corresponding extraction during ice formation is ignored. If sea-ice concentrations are considered as different from zero, the water mass decomposition analysis will yield much larger meteoric fractions as a consequence [e.g., *Guay et al.*, 2009]. Furthermore, the effects of extraction and release of the above compounds on our analysis is so small as to be negligible for our purposes. The Ba concentrations in the Horton River Estuary are similar to those reported for other North American rivers [e.g., *Guay and Falkner*, 1998; *Cooper et al.*, 2008]. If we assume that there is only minor seasonal variability in the riverine Ba concentrations [*Guay and Falkner*, 1998], the Horton River Ba concentration (295 nM Ba, Table 1) is close to the flow-weighted average concentrations of the nearby Mackenzie (371 nM Ba) or Yukon (369 nM Ba) Rivers [*Cooper et al.*, 2008].

[15] Using the fractions of the individual components F_{SW} , F_{SIM} and F_{UHL} , we computed the “ideal” Ba concentrations (Ba_{ideal}) in the upper water column down to $S_p = 33.1$, as outlined above.

$$F_{MW}Ba_{(MW)} + F_{SIM}Ba_{(SIM)} + F_{UHL}Ba_{(UHL)} = Ba_{ideal} \quad (5)$$

Table 1. End-Members and Characteristics Used for the Water Mass Decomposition Analysis^a

	A_T ($\mu\text{mol kg}^{-1}$)	Salinity (S_p)	Ba (nM)	$\delta^{18}\text{O}$ (‰)
Meteoric water	1880.0	0	295	-20
Sea-ice melt	0	0	0	-2.0
Upper Halocline water	2283.0	33.1	69	-1.5

^aAll data were measured during our cruises. The meteoric water concentrations were measured in the Horton River Estuary during our program in spring 2008. $\delta^{18}\text{O}$ for sea-ice melt is adapted from Bates *et al.* [2009]. Salinity and A_T were used in the decomposition analysis, whereas Ba was used to compute the “ideal” Ba concentrations. Note that values quoted below may differ from those used in other studies [Chierici *et al.*, 2011] in the same area because of spatial and temporal variability. Furthermore, the null salinity and alkalinity ascribed to the sea-ice melt-water reflect the integrated annual effect of the ice cycle.

[16] Ba_{ideal} represents the expected Ba concentration if Ba was a conservative property. For each sample, the difference between the actual, i.e., observed Ba concentration (Ba_{obs}), and Ba_{ideal} is used to compute the Ba deficiency, which we attributed to Ba export (Ba_{exp}) from the surface layer due to sinking of bio-Ba. In the discussion that follows we adopt a ratio of $C_{\text{org}}:\text{bio-Ba} = 225 \text{ g C (g Ba)}^{-1}$ [2575 mol C (mol Ba)⁻¹], an approximate average of the values reported by Dymond *et al.* [1992], Broecker and Peng [1982], and Francois *et al.* [1995]. The estimate by Broecker and Peng [1982], ($C_{\text{org}}:\text{bio-Ba} = 260 \text{ g C (g Ba)}^{-1}$), served as an upper bound, whereas values of $C_{\text{org}}:\text{bio-Ba} = 185\text{--}200 \text{ g C (g Ba)}^{-1}$ compiled by Dymond *et al.* [1992] are at the lower limit, with the value of $C_{\text{org}}:\text{bio-Ba} = 215 \text{ g C (g Ba)}^{-1}$ reported by Francois *et al.* [1995] ranging in between. The

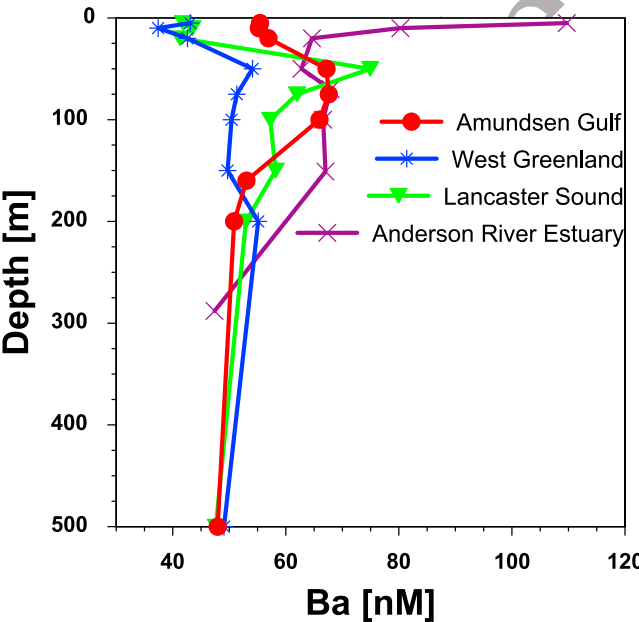


Figure 3. Dissolved Ba profiles from selected stations in the Canadian Arctic Archipelago and Baffin Bay. Individual dissolved Ba profiles are shown for four locations: the Mackenzie Shelf (purple line), the Amundsen Gulf (red line) and Lancaster Sound (green line), as well as near the west Greenland Coast (blue line). Please refer to insert for locations.

subsequent Ba inventory and carbon flux assessments were computed for the upper 50 m of the water column.

3. Results and Discussion

3.1. Spatial Variability of Dissolved Ba Concentrations

[17] Profiles from selected stations across the CAA show (Figure 3) the lowest Ba concentrations ($\sim 40 \text{ nM}$) in the surface waters of eastern Baffin Bay and in the outflow of Lancaster Sound into Baffin Bay. The Ba profile recorded in the Amundsen Gulf (Figure 3) displays a nutrient-type pattern with surface water concentrations of approximately 50–60 nM Ba. The high Ba concentrations (65–70 nM Ba) in the subsurface waters of the CAA (Figures 3 and 4) correspond to an eastward flowing water mass [e.g., Shadwick *et al.*, 2011a] with a core salinity of 33.1, that is characteristic of the Pacific or Upper Halocline water mass. Irrespective of our sampling location, whether on the eastern or western side of the CAA, Ba concentrations converge to approximately 48 nM Ba in the deeper waters of Atlantic origin. In the western-most profile, at a near-shore station close to the Anderson River Estuary, Ba concentrations are elevated by runoff in the near surface layer but also display nutrient-like characteristics in the subsurface waters. In the surface waters of the eastern part of the CAA, the westward intrusion of water from Baffin Bay is

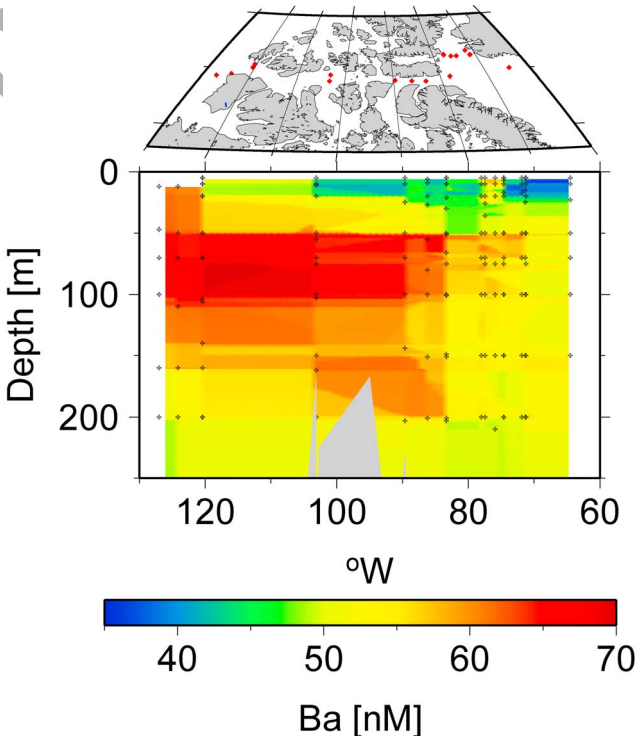


Figure 4. Distribution of dissolved barium in the Canadian Arctic Archipelago. We show the distribution of dissolved Ba along 75°N from the eastern Beaufort Sea to Baffin Bay and a subsequent cross section through Nares Strait. Please note the different Ba characteristics on the eastern (west of approximately 70°W, [Ba] $\approx 45 \text{ nM}$) and western (east of approximately 80°W, [Ba] $\approx 55 \text{ nM}$) sides of Nares Strait.

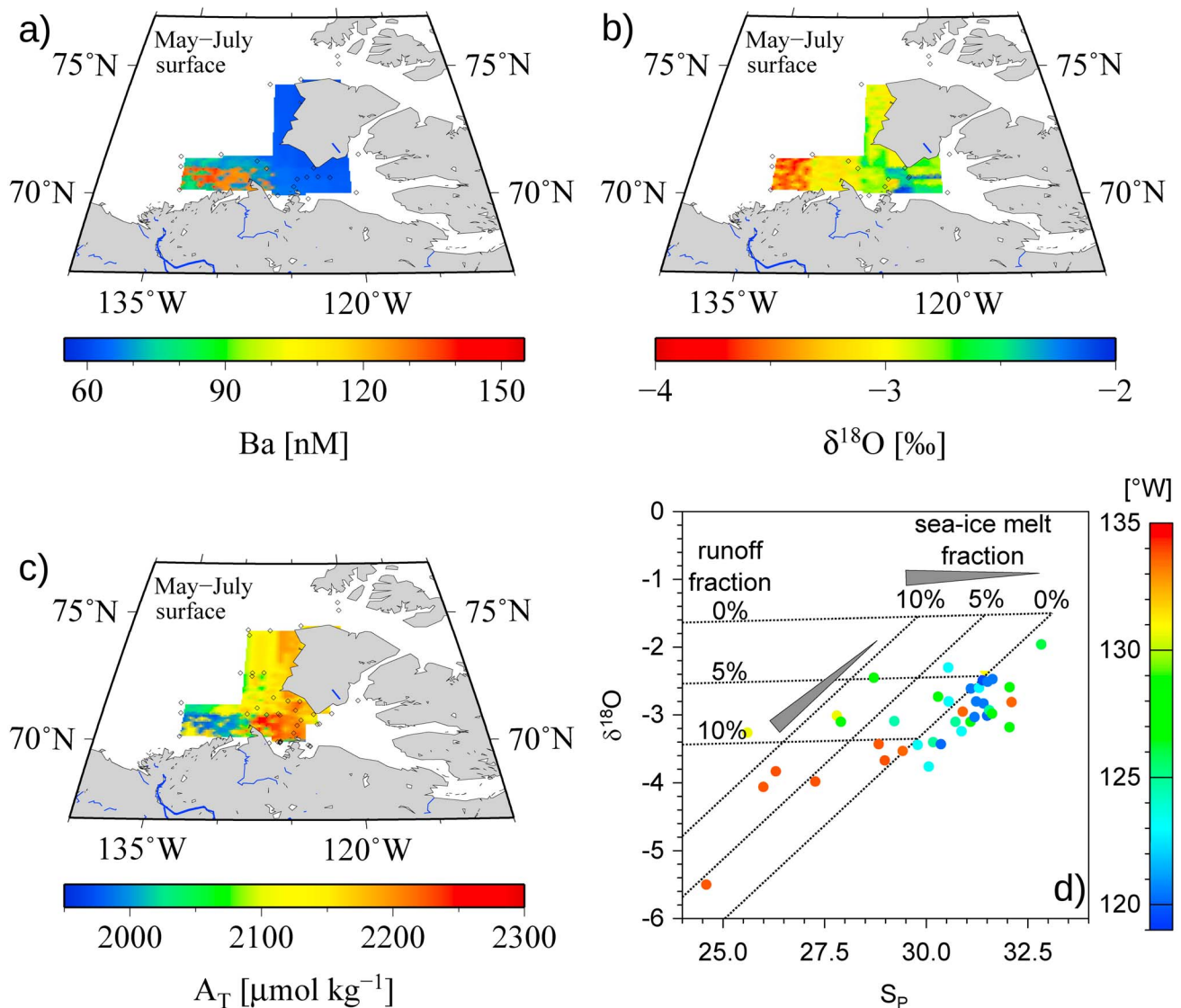


Figure 5. Distribution of Ba, $\delta^{18}\text{O}$, and A_T during Spring 2008. (a) Dissolved Ba, (b) $\delta^{18}\text{O}$, and (c) A_T in surface waters are shown as average observations made during the months of May, June, and July 2008. The elevated Ba and lower A_T concentrations near the mouth of the Anderson River correspond to more negative $\delta^{18}\text{O}$ values [e.g., Bates *et al.*, 2009]. (d) Following Macdonald *et al.* [1989] and Bates *et al.* [2009], freshwater from river runoff and sea-ice melt are distinguished on the basis of their salinity and $\delta^{18}\text{O}$ characteristics. The color coding in Figure 5d indicates the longitude of the sampling location.

evident from the low Ba concentrations (Figure 4). It is also interesting to note the presence of the northward flowing West Greenland Current [e.g., Münchow and Melling, 2008], waters of Atlantic origin, characterized by low dissolved Ba concentrations, on the eastern side of Nares Strait (Figure 4). The southward flowing waters on the western side of Nares Strait originate from the Arctic and are characterized by relatively high Ba concentrations, since the Arctic Ocean serves as collector for Arctic river water with elevated Ba concentrations [e.g., Guay and Falkner, 1998; Cooper *et al.*, 2008].

[18] After the ice breakup in late April and early May, river runoff affects the surface waters, in particular in the

western part of the study area (Figure 5). The surface salinity minimum caused by both river runoff and sea-ice melt is usually observed in September, corresponding to the minimum sea-ice coverage [e.g., Shadwick *et al.*, 2011b]. In spring, i.e., during the months of May through July, we observed high dissolved Ba concentrations in nearshore areas, increasing in the westerly direction (Figure 5a) caused by the arrival of riverine freshwater with high Ba concentrations. The early arrival of freshwater from rivers (compared to sea-ice melt) is also evident from the distribution of $\delta^{18}\text{O}$ in the mixed layer. Sea-ice $\delta^{18}\text{O}$ -values are approximately -2‰ [Bates *et al.*, 2009], therefore the significantly more negative values recorded in the surface

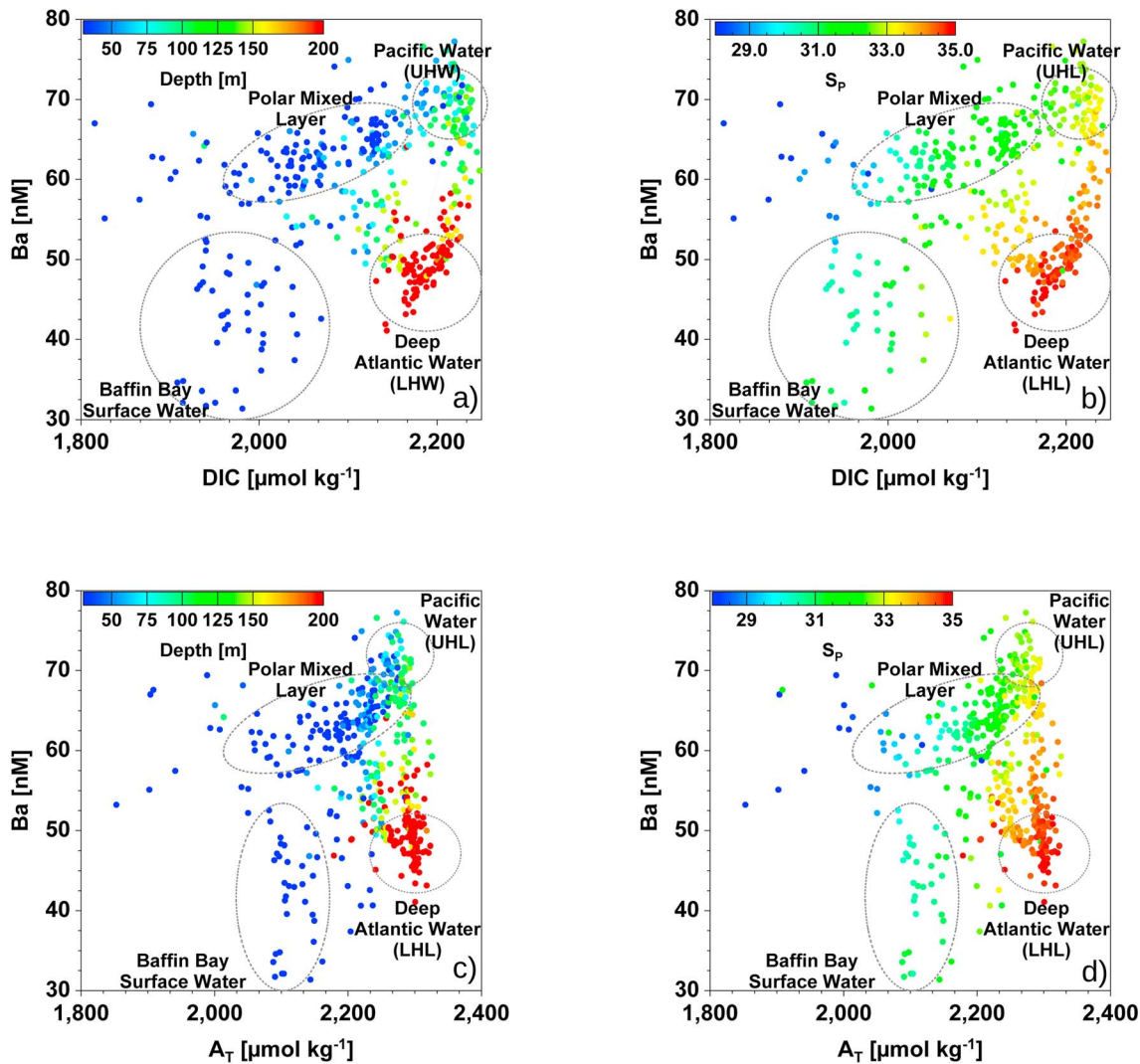


Figure 6. Relationship between carbonate system parameters and Ba. (a, b) Ba versus DIC and (c, d) Ba versus A_T are shown with corresponding depth (Figures 6a and 6c) or salinity (Figures 6b and 6d) values in color. The color coding does not reveal the full ranges of depth or salinity, but focuses on the 30–200 m depth range, where the gradients are strongest. Higher or lower values of salinity and depth are included within the maximum/minimum color, respectively. The lines are drawn to underline the conservative behavior of Ba and A_T in the deeper waters, in contrast to DIC, which clearly reveals the addition of metabolic CO_2 as shown by *Shadwick et al.* [2011a, 2011b]. The Pacific and deep Atlantic water masses are also called Upper and Lower Halocline Waters (UHL, LHL), respectively.

394 mixed layer in the western part of our study area ($\sim 4\%$)
 395 reflect inputs from runoff with a $\delta^{18}\text{O}$ signature of approx-
 396 imately -20% [Macdonald et al., 1989; Cooper et al., 2008;
 397 Bates et al., 2009; Yi et al., 2010] (Figure 5b). As a con-
 398 sequence of the arrival of riverine freshwater, A_T decreases
 399 in the western areas (Figure 5c), since riverine A_T con-
 400 centrations are lower than A_T concentrations of the
 401 Amundsen Gulf [e.g., *Shadwick et al.*, 2011a]. At this time
 402 of the year (May–July), our observed $\delta^{18}\text{O}$ composition of
 403 the surface waters, which is in good agreement with the
 404 above mentioned literature values, reveals little or no con-
 405 tribution by fresh water from sea-ice melt, whereas the
 406 runoff fraction clearly increases in the westerly direction
 407 (Figure 5d). The spatial distribution of the $\delta^{18}\text{O}$ composi-
 408 tion in surface waters shows a clear east to west gradient

(Figure 5b) with values at -2% in the Amundsen Gulf indi-
 409 cating a low influence of river runoff here, and more negative
 410 values of -4% in the western part close to the estuaries. This
 411 agrees with findings by *Magen et al.* [2010], *Shadwick et al.*
 412 [2011a], and *Cheirici et al.* (submitted manuscript, 2011), that
 413 little or no runoff from the Mackenzie or Horton rivers
 414 reaches the Amundsen Gulf at any time of the year.
 415

[19] The relationship between dissolved Ba and DIC
 416 exposes two distinctly different regimes: the waters above
 417 and below the UHL (Figures 6a and 6b). Within the Polar
 418 Mixed Layer (PML), a mixture of SIM, MW and UHL,
 419 covering approximately the upper 50 m of the water column
 420 and with a S_p range between 29.5 and 31, the concentra-
 421 tions of Ba and DIC are positively correlated and increase
 422 with depth until they reach values similar to those in the
 423

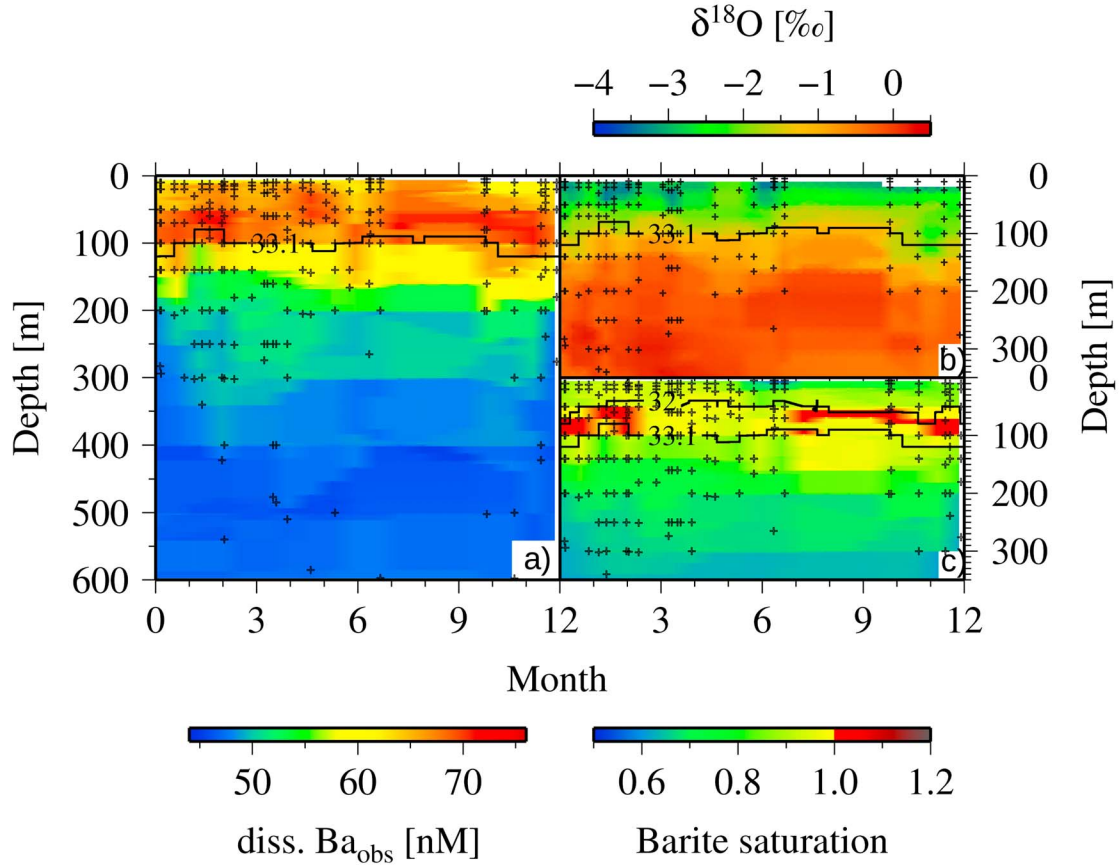


Figure 7. Temporal evolution of Ba, $\delta^{18}\text{O}$, and the barite saturation state in the Amundsen Gulf. (a) The dissolved Ba concentrations for the water column of the Amundsen Gulf. (b and c) We show $\delta^{18}\text{O}$ and the barite saturation state. We indicate the $S_p = 33.1$ isopleth, as well as the $S_p = 32$ isoline in Figure 7c, both encompassing approximately the depth range of 50 m to 100 m.

subsurface waters (50–100 m). Dissolved Ba concentrations are highest just above the UHL, originating from the Pacific at $S_p = 33.1$ (see also discussion in section 3.2.), while DIC continues to increase below the UHL due to the respiration of settling organic matter. Finally, both DIC and Ba concentrations decrease in deeper waters (Figure 6a) as Atlantic Ocean Water is encountered. The A_T/Ba relationships (Figures 6c and 6d) exhibit similar patterns to the DIC/Ba relationships, but given the more conservative behavior of A_T , relative to DIC, stronger linear correlations are observed in the sub-halocline waters. The addition of metabolic DIC occurs at timescales that are shorter or similar to the residence time of the subsurface waters in the Amundsen Gulf (1–2 years [Lanos, 2009]; see also below section 3.4.), while the release of A_T and the dissolution or formation of barite occurs over longer, multiyear time scales, such that the A_T/Ba relationship appears to be dominated by water mass mixing (Figure 6d).

[20] We computed the Ba outflow from the Canadian Archipelago via Lancaster Sound in order to compare our observations with those of Taylor *et al.* [2003]. According to Ingram [2002; see also Shadwick *et al.*, 2011a], the outflow from Lancaster Sound into Baffin Bay is on the order of $1.1 \cdot 10^6 \text{ m}^3 \text{ s}^{-1}$. Using this estimate, a depth-

weighted water column average Ba concentration of 51.2 nM Ba (Figure 3), and a water column depth of 500 m, yields an annual dissolved Ba export from the CAA into Baffin Bay on the order of $1.6 \cdot 10^9 \text{ mol Ba yr}^{-1}$ or $222 \cdot 10^9 \text{ g Ba yr}^{-1}$ ($56.3 \text{ mol Ba s}^{-1} / 7.7 \cdot 10^3 \text{ g Ba s}^{-1}$, respectively). Taylor *et al.* [2003] reported an outflow from the Canadian Archipelago of $89.7 \pm 7.6 \text{ mol Ba s}^{-1}$. Our estimate is smaller but of the same order of magnitude. Taylor *et al.* [2003] also considered the outflows from Jones Sound, Smith Sound, and Barrow Strait, whereas our estimate is restricted to the contribution from Lancaster Sound. Furthermore, it is worth noting that our depth-weighted average Ba concentration for Lancaster Sound (51.2 nM Ba) is slightly lower than the value reported by Taylor *et al.* [2003] ($62.4 \pm 5.1 \text{ nM Ba}$).

3.2. Dissolved Ba and Barite Solubility in the Amundsen Gulf

[21] We now investigate the temporal evolution of dissolved Ba concentrations and of the saturation state of the waters with respect to barite (BaSO_4) in the Amundsen Gulf (Figures 7–9). The barite saturation state is expressed as:

$$\text{Saturation state} = \frac{Q_{(\text{BaSO}_4, \text{aq})}}{K_{Sp}(\text{Barite})} \quad (6)$$

where $Q_{(\text{BaSO}_4, \text{aq})}$ is the ion activity product of aqueous barium sulphate and $K_{\text{sp}}(\text{Barite})$ is the thermodynamic solubility product of barite [Monnin, 1999]. The $\text{BaSO}_4(\text{aq})$ ion activity product can be expressed as

$$Q_{(\text{BaSO}_4, \text{aq})} = m_{\text{Ba}^{2+}(\text{t}, \text{aq})} \cdot m_{\text{SO}_4^{2-}(\text{t}, \text{aq})} \cdot \gamma_{\text{BaSO}_4(\text{t}, \text{aq})}^2 \quad (7)$$

where m is the total molality of the designated aqueous species and γ is the total (or stoichiometric) mean activity coefficient of aqueous barium sulphate in seawater. The various thermodynamic quantities are calculated after Monnin [1999]. This model has been used to investigate the saturation state of the global ocean from the GEOSECS data [Monnin et al., 1999]. A full description of the calculation of the barite saturation state from the measured quantities (dissolved Ba concentration, temperature, S_p and depth) is given by Hoppema et al. [2010].

[22] As indicated in Figure 3, dissolved Ba surface water concentrations are approximately 65.2 ± 2.4 nM Ba in the upper 50 m of the Amundsen Gulf, and nearly invariant throughout the year, except for a slight decrease during the later part of the year (Figure 7a). Within the subsurface layer, bounded by the SML and the $S_p = 33.1$ isopleth, the dissolved Ba concentrations reach maximum values of approximately 68.5 ± 2.0 nM Ba. Here, as well, the

concentrations appear to be relatively constant throughout the year (Figure 7a). Below the UHL, the influence of deeper waters of Atlantic origin is reflected by decreasing Ba concentrations with depth to minimum values of approximately 45 nM Ba (Figure 7a, 48.1 ± 1.9 nM Ba below 200 m; 47.4 ± 0.9 nM Ba below 300 m). The stable oxygen isotope composition of water (Figure 7b) reveals lowest values of approximately $\delta^{18}\text{O} = -3.6\text{‰}$ in the surface layer ($-2.7 \pm 0.4\text{‰}$ average in the upper 50m), and more positive values with depth to approximately $\delta^{18}\text{O} = -1.5\text{‰}$ in the UHL layer at $S_p = 33.1$ ($-1.7 \pm 0.4\text{‰}$ average between 50m and 100m), and most positive values of $\delta^{18}\text{O} = 0.76\text{‰}$ in the deep Atlantic layer ($0.0 \pm 0.3\text{‰}$ average below 200m, $0.0 \pm 0.3\text{‰}$ average below 300m, $0.3 \pm 0.3\text{‰}$ average below 500m).

[23] In order to distinguish between the two major processes, that shape the nutrient-type barium profile: (1) the release of Ba from decaying organic matter in the layer just below the euphotic zone, and (2) the mixing of the surface and subsurface water masses, we consider the saturation state of the waters with respect to barite (Figure 7c). The surface waters, i.e., the upper 50 m of the water column, are undersaturated with respect to barite throughout the year, particularly in June, which coincides with the maximum in net community production (NCP) [Shadwick et al., 2011b] (see also discussion in section 3.3); yet closer to saturation during ice-covered winter months than during the ice-free season. In the subsurface layer, between 50 m and 100 m depth, the saturation state values reach a maximum with barite saturation observed between June and February. This

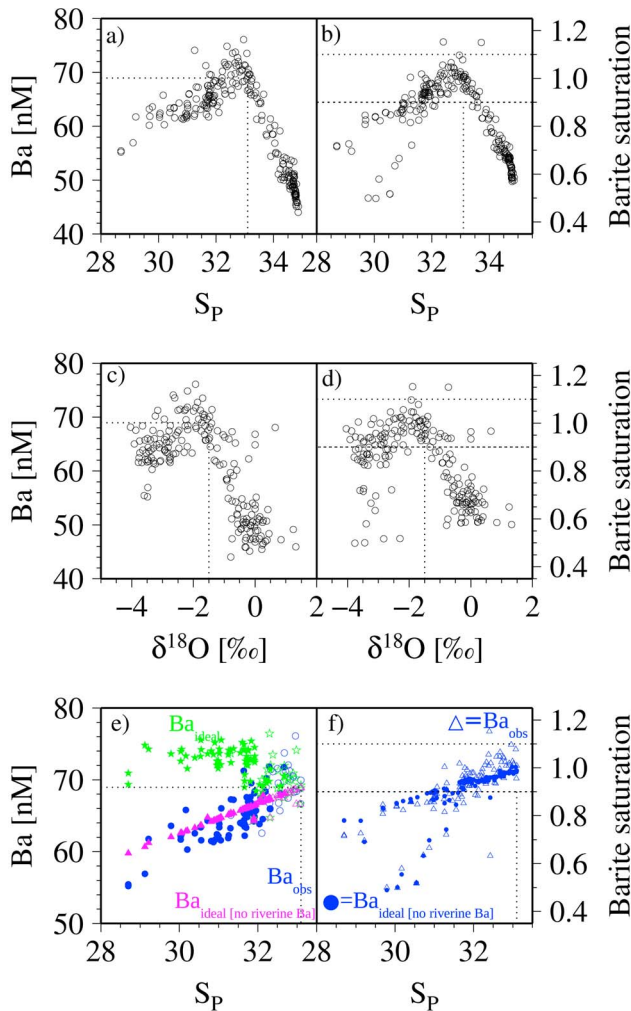


Figure 8. Property/property plots of Ba related and hydrographic parameters observed in the Amundsen Gulf. For the entire water column in the Amundsen Gulf, the relationships of dissolved Ba and the saturation state of barite (a, b) versus salinity and (c, d) versus $\delta^{18}\text{O}$ are shown. (e, f) Excerpts are shown for the upper part of the water column, i.e., for all samples with $S_p \leq 33.1$ (see Figure 2). Observed dissolved Ba concentrations (Ba_{obs}) are shown (blue dots), as well as the ideal Ba concentrations according to the three end-member mixing model (green diamonds). Furthermore, the model was run without riverine Ba ($\text{Ba}_{\text{ideal}}\{\text{no Ba}_{\text{river}}\}$, magenta triangles), which represents a conservative mixing between surface waters and UHL. The difference between Ba_{obs} and Ba_{ideal} (Ba deficiency) is attributed to Ba export (Ba_{exp}) via sinking of organic matter (i.e., as bio-Ba). The conservative behavior of $\text{Ba}_{\text{ideal}}\{\text{no Ba}_{\text{river}}\}$ clearly emphasizes the importance of riverine Ba contributions to the surface layer Ba concentrations. Samples deeper than 50 m are plotted as open symbols, while shallower samples are plotted as solid symbols (Figure 8e). For samples with $S_p \leq 33.1$ we compare the observed barite saturation state (open symbols) with the barite saturation state computed with $\text{Ba}_{\text{ideal}}\{\text{no Ba}_{\text{river}}\}$. The Ba surplus at $S_p > 32$ is attributed to the decay of bio-Ba (Figure 8f). Please note that no river contribution can be detected below 50 m, approximately corresponding to $S_p > 32$ (see also Figure 7c). The dotted lines in all panels indicate the properties of the UHL waters (Table 1), and/or the equilibrium level of the barite saturation = 0.9–1.1, which inherently assumes an uncertainty of 10% in the computation of the barite saturation state [Monnin et al., 1999].

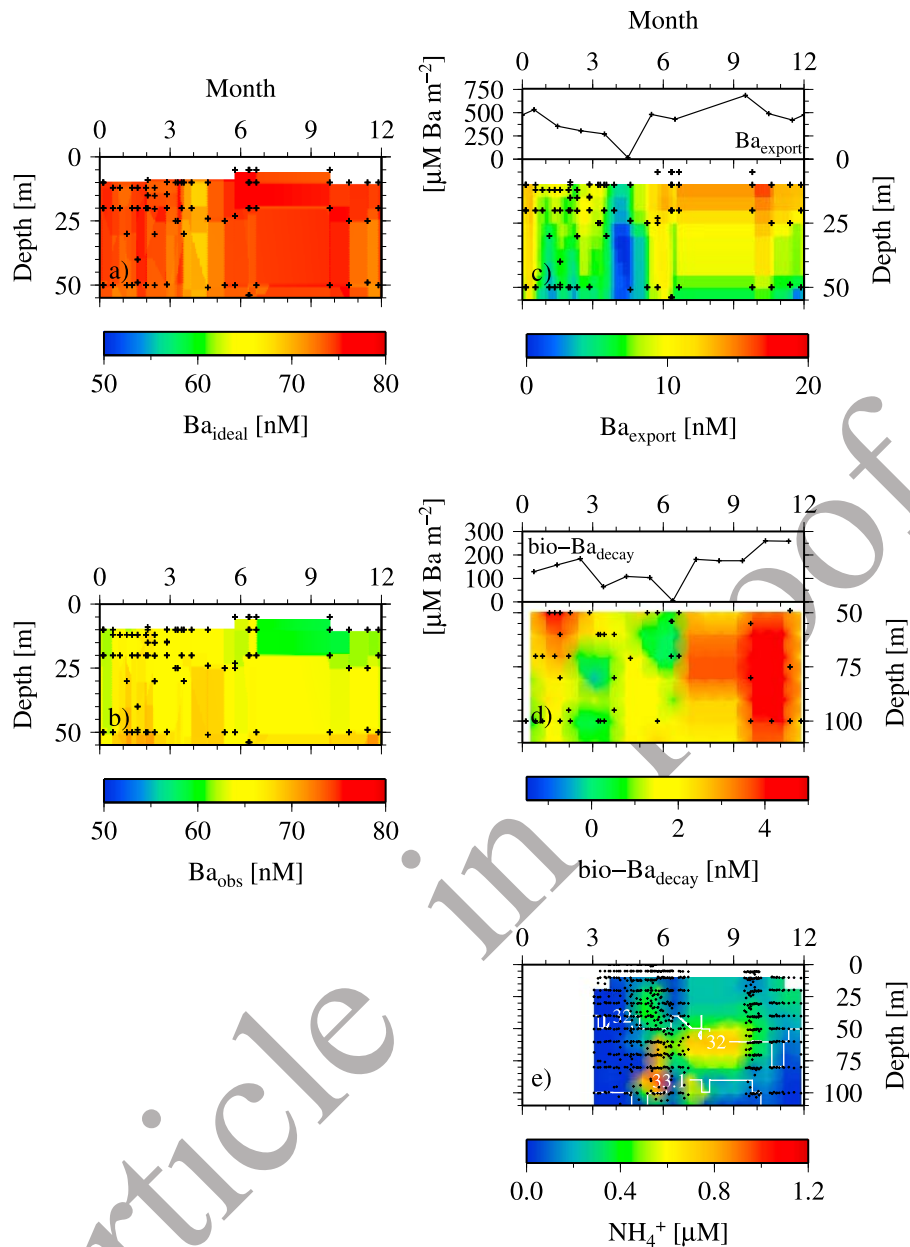


Figure 9. Time series of Ba_{ideal} , Ba_{obs} , Ba_{export} , decay of bio-Ba, and NH_4^+ for Amundsen Gulf. The seasonality of (a) Ba_{ideal} , (b) Ba_{obs} , and (c) Ba_{exp} for the upper 50 m of the water column in Amundsen Gulf is shown for a full annual cycle. Please note the change in the color scale in Figure 9c. We computed the decay of bio-Ba in the subsurface layer of the Amundsen Gulf as difference from the observations and the assumed conservative mixing between the surface layer and the UHL (lower panel, see also Figure 8f). The upper panel shows the integration of this Ba surplus over the depth range of 50 m to 100 m, i.e., approximately over the S_p range 32–33.1. For comparison, we show the seasonal evolution of NH_4^+ in the upper water column of Amundsen Gulf. NH_4^+ can be considered as a tracer of respiratory activity, thus indicating the arrival of sinking particulate organic matter and the onset of its respiration in the subsurface layer [see also *Forest et al.*, 2011].

519 layer is undersaturated with respect to barite only during the
 520 winter months before the onset of NCP in the surface layer.
 521 To summarize, the highest barite saturation states are found
 522 between the $S_p = 32$ isopleth at approximately 50 m water
 523 depth and the $S_p = 33.1$ isopleth corresponding to the UHL
 524 (Figure 7c), i.e., between the bottom of the surface mixed
 525 layer and the UHL. In the open ocean the bottom of the

surface mixed layer typically corresponds to the depth of
 maximum respiration rates [e.g., *Aristegui et al.*, 2005].
 527 The Amundsen Gulf is a shelf system and, clearly, is shal-
 528 lower than the open ocean, but nevertheless the maximum
 529 of respiratory activity, as indicated by the maximum of
 530 the ammonium concentrations (Figure 9e), and the highest
 531 barite saturation states coincide with the bottom of the
 532

surface layer. The occurrence of a barite saturation state maximum is best visualized in property/property plots of selected hydrographic parameters and dissolved Ba concentrations or the barite saturation state (Figure 8). The dissolved Ba versus salinity relationship highlights two distinct sections, each with nearly conservative behavior. A positive correlation of Ba and salinity is observed above the $S_p = 33.1$ horizon. While the $S_p = 33.1$ layer is characterized by an average Ba concentration of 69 nM Ba (Table 1), the maximum Ba concentration is actually found at lower salinities, thus above the $S_p = 33.1$ isopleth. Below the $S_p = 33.1$ isopleth, dissolved Ba concentrations decrease with increasing salinity reaching a minimum in the deep waters of Atlantic origin (Figure 8a). Similarly, the highest dissolved Ba values, and the only barite-equilibrated waters, are observed above the depths of the 33.1 isopleth (Figure 8b) between approx. 50 m and 100 m depth (Figure 7c). Above and below this level the water column is undersaturated with respect to barite. The group of particularly low barite saturation states at salinities of 30–31 is associated with warm waters in July [see, e.g., *Shadwick et al.*, 2011b, Figure 6b]. Similar features arise when plotting dissolved Ba concentrations or the barite saturation state versus $\delta^{18}\text{O}$: the $\delta^{18}\text{O}$ signature of the $S_p = 33.1$ isopleth is approximately $\delta^{18}\text{O} = -1.5\text{‰}$ (Table 1), while both the dissolved Ba concentrations and the barite saturation state maximum correspond to values of $\delta^{18}\text{O} \approx -2\text{‰}$ (Figure 8c and 8d). Using the results of the subsequent water mass decomposition analysis down to the S_p level of 33.1 as a composite of MW, SIM, and UHL water (see equation (2)), we provide further evidence for the enrichment of dissolved Ba above the $S_p = 33.1$ layer. If we assume, as a thought experiment, that the meteoric Ba concentrations are zero (i.e., $\text{Ba}_{\text{ideal}}\{\text{no Ba}_{\text{river}}\}$) as detailed in the following section, the Ba versus salinity relationship becomes conservative and reflects a linear mixing of the PML and UHL waters (Figures 8e and 8f). If we compare these results with our measurements, we see that in the salinity range between $S_p = 32$ and $S_p = 33.1$ the observed Ba concentrations and the barite saturation state appear elevated relative to the conservative Ba (i.e., $\text{Ba}_{\text{ideal}}\{\text{no Ba}_{\text{river}}\}$) versus S relationship. In fact, the only values corresponding to barite saturation correspond to those that deviate from the linear Ba versus S relationship between the $S_p = 32$ and $S_p = 33.1$ (see open circles and triangles in Figures 8e and 8f). Since the contribution of MW to subsurface waters is negligible, we attribute the dissolved Ba surplus in the subsurface layer within the 32 to 33.1 S_p range to the release of Ba from decaying organic matter ($\text{bio-Ba}_{\text{decay}}$), which sank out of the surface layer (Figures 9c and 9e). This Ba surplus peaks in late autumn, coinciding with the accumulation of dissolved organic carbon (DOC) and DIC in this subsurface layer in response to organic matter decay [see *Shadwick et al.*, 2011b, Figures 8c and 8d]. Integrating this Ba surplus over the 50–100 m depth range yields a maximum Ba release of approximately 260 μM Ba m^{-2} (Figure 9c), corresponding to approximately 40% of the bio-Ba formed in the surface layer (Figure 10). The degradation of settling organic matter and the concomitant release of Ba to the water column explains the nutrient-like behavior of dissolved Ba. A further, biologically mediated process affecting dissolved Ba concentrations is the precipitation of barite, which is associated with enhanced respiratory activity [e.g., *Dehairs et al.*, 1992]. This process, however, cannot be

detected in our dissolved Ba measurements, since the amount of barite precipitation is approximately three orders of magnitude lower than the bio-Ba turnover.

3.3. Variability of Ba in the Amundsen Gulf and Export of Ba out of the Surface Layer

[24] In order to arrive at an annual budget for dissolved Ba for the Amundsen Gulf area (Figure 1), we employ a three end-member mixing model for the upper water column. The three end-members are meteoric water, sea-ice meltwater and Upper Halocline Water, as defined by their respective A_T , salinity and $\delta^{18}\text{O}$ values (Table 1). The model yields the temporal evolution of their respective fractions over the course of the year. The maximum SIM contribution was 10% in October, whereas MW reached a maximum at 5% in the spring. Compared to the analysis of *Guay et al.* [2009], our values are higher for SIM and lower for MW, respectively. This discrepancy may reflect both a seasonal bias, as *Guay et al.* [2009] sampled only in summer during the salinity minimum, and the assumption that sea-ice constitutes a net annual source of salt. As noted previously this assumption is only valid at a seasonal time scale and at an appropriate spatial scale.

[25] On the basis of the above mixing analysis, we computed “ideal” Ba concentrations (Ba_{ideal}) (equation (5)) under the assumption that dissolved Ba behaves conservatively. In order to highlight the role of riverine dissolved Ba, we also show the observed Ba (Ba_{obs}), together with Ba_{ideal} and $\text{Ba}_{\text{ideal}}\{\text{no Ba}_{\text{river}}\}$, the latter computed under the assumption that the MW does not carry any dissolved Ba (Figures 8e and 8f). The $\text{Ba}_{\text{ideal}}\{\text{no Ba}_{\text{river}}\}$ displays a near perfect conservative relationship to salinity, but it clearly underestimates Ba_{obs} . The riverine Ba contributed up to 15% of the Ba inventory in the upper 50 m of the water column (Figure 10a). We attribute the deficiency between Ba_{obs} and Ba_{ideal} to Ba export (mainly as bio-Ba) out of the surface layer (Ba_{exp} , Figure 8e) and computed Ba_{exp} for each observation throughout the annual cycle (Figures 9 and 10). The Ba deficiency in the surface layer and thus Ba_{exp} peaked in late summer/early autumn, when biological activity waned. The Ba_{exp} was lowest during the salinity maximum in late winter, just before the onset of increased biological activity triggered by longer daylight hours and ice melt, and shortly before the delivery of significant amounts of riverine Ba. In the subsurface layer below 50 m, Ba_{ideal} and Ba_{obs} are more similar (i.e., $\text{Ba}_{\text{exp}} = 0$), indicating that the bio-Ba is primarily formed in, and exported from, the euphotic zone. The onset of the Ba export out of the surface layer (Figure 9c) is nicely mirrored by the rise of the ammonium (NH_4^+) concentrations [Forest et al., 2011] in the subsurface layer (Figure 9e), interpreted as an indicator of the arrival of sinking organic matter and is subsequent respiration. The high turnover rates of NH_4^+ prevent its accumulation in the water column, in contrast to the build-up of the Ba deficiency in the surface layer throughout the seasons. Within the subsurface layer, the build-up of the bio- Ba_{decay} (Figure 9d) occurs somewhat delayed with respect to the onset of the Ba deficiency in the surface layer (Figure 9c) and the beginning of enhanced NH_4^+ concentrations in the subsurface layer (Figure 9e). On the other hand, as mentioned above, the rise of bio- Ba_{decay} appears concomitant to the increase of DOC concentrations in the subsurface layer [*Shadwick et al.*, 2011b, Figure 8d],

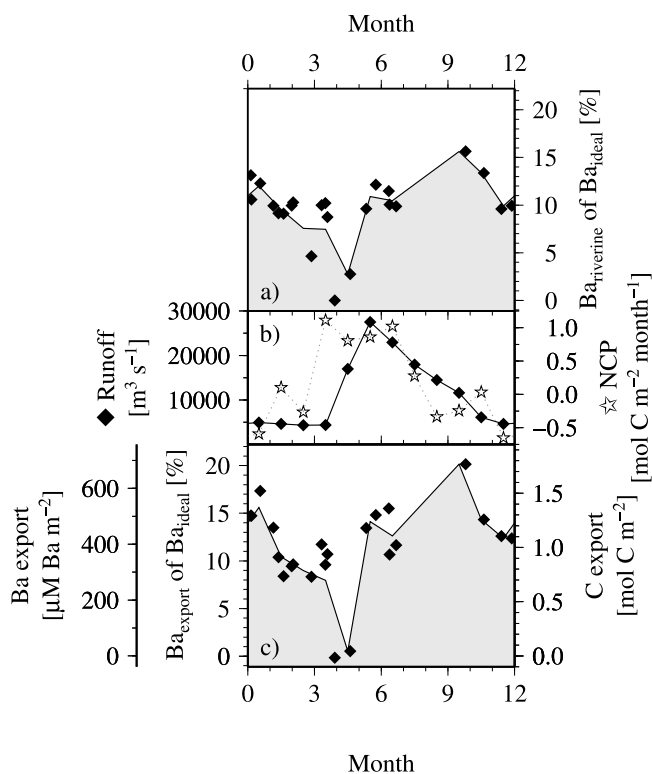


Figure 10. Temporal evolution of Ba-related inventories in the upper 50 m of the water column. (a) The fraction of riverine Ba, which is exported. (b) The temporal evolution of river runoff and NCP (NCP after Shadwick *et al.* [2011b] and river runoff after Prange [2002]; see also Water Survey of Canada, http://www.wsc.ec.gc.ca/staflo/index_e.cfm?cname=flow_daily.cfm). (c) Export of Ba and derived carbon export are shown as well as the fraction of Ba_{ideal} , which is exported. Squares indicate individual data, whereas shaded areas represent the monthly averages (Figures 10a and 10c). The lowest fraction of riverine Ba (Figure 10a) coincided with the salinity maximum, and the highest fraction with the salinity minimum. Increased Ba export (Figure 10c) coincided with the under-ice algal bloom, slightly earlier than the arrival of riverine freshwater (Figure 10b). Ba export exceeded the riverine Ba inputs. Ba and carbon exports peak in late summer, at the end of the biologically active period (Figure 10b).

as both originate from the decay of organic matter, and both are more stable than NH_4^+ . The sinking rates of organic particles vary over a wide range, from a few meters to a few hundred meters per day [e.g., Kellogg *et al.*, 2011; Armstrong *et al.*, 2009]. Assuming slowly sinking particles with sinking rates $<3 \text{ m d}^{-1}$, as reported for the investigation area [Kellogg *et al.*, 2011], the settling time would be on the order of 1–2 months. This would be in general agreement with the findings discussed here, such as the delay between the rise of Ba_{exp} and bio- Ba_{decay} in the surface and subsurface layers, respectively (Figures 9c and 9d).

3.4. Export Production of Carbon

[26] We estimated the export of particulate organic carbon from the surface layer by assuming that it is tightly related to

the bio-Ba flux [e.g., Bishop, 1988; Dehairs *et al.*, 1992, 1997; Dymond *et al.*, 1992; Francois *et al.*, 1995; Dymond and Collier, 1996; Gillikin *et al.*, 2006; Sternberg *et al.*, 2007; Calvert and Pederson, 2007] and that the latter can be computed from the dissolved Ba deficiencies in the upper 50 m of the water column (Figure 8e). We employed an average ratio of $C_{org}:bio-Ba = 225 \text{ g C (g Ba)}^{-1}$ [2575 mol C (mol Ba) $^{-1}$], adopted from Dymond *et al.* [1992], to estimate the export of particulate organic carbon from the surface layer. Our results indicate that the bio-Ba and organic carbon export fluxes from the upper 50 m of the water column (Figure 10b) were smallest toward the end of winter ($\sim 0.3 \text{ mol C m}^{-2}$), before the onset of biological activity led by the proliferation of ice and under ice algae, when ice cover still persisted [e.g., Horner and Schrader, 1982; Lavoie *et al.*, 2009]. River runoff and the associated supply of riverine Ba lag behind the increase in Ba_{exp} (Figure 10b), highlighting the contribution of ice algae and under-ice algae to the initial spring export of organic carbon out of the surface layer. The time lag between the onset of export production and the increased (under ice) carbon fixation, i.e., of net community production (NCP) [see Shadwick *et al.*, 2011b], is consistent with the seasonal evolution of biological activity in the Canadian Arctic [Horner and Schrader, 1982; Carmack *et al.*, 2004; Lavoie *et al.*, 2009]. NCP remains high after the peak river discharge, but wanes in late summer, when heterotrophic processes begin to out-compete organic matter production. Around September, the export of organic matter, i.e., Ba_{exp} , reaches its maximum. From the perspective of the dissolved Ba pool, the riverine Ba was efficiently captured by bio-Ba formation, since the “new” Ba arrived just when biological activity was highest (Figure 10b). This may explain the lack of strong seasonality in dissolved (observed) Ba (Figure 9b) profiles, as Ba_{exp} and $Ba_{riverine}$ displayed a similar seasonality (Figures 10a, 10b, 9a, and 9c), but with opposing effects on Ba_{obs} . Assuming that Ba_{exp} integrates the organic carbon export at the annual scale, the Ba_{exp} maximum corresponds to an annual organic carbon export of approximately $1.8 \text{ mol C m}^{-2} \text{ yr}^{-1}$. Since estimates of primary productivity span over a rather wide range ($4.4 \pm 1 \text{ mol C m}^{-2} \text{ yr}^{-1}$, assuming that this result, obtained by Forest *et al.* [2011] for the period March–August, is representative for the entire year; $7\text{--}15 \text{ mol C m}^{-2} \text{ yr}^{-1}$, based on satellite data [Arrigo and van Dijken, 2004]), and particle export studies cover only parts of the annual cycle [Forest *et al.*, 2011; Magen *et al.*, 2010], their relationship to our findings cannot readily be appreciated. Nevertheless, our estimated carbon export ($1.8 \text{ mol C m}^{-2} \text{ yr}^{-1}$) would represent 12–40% of the estimated primary production [Arrigo and van Dijken, 2004; Forest *et al.*, 2011], which is in a reasonable range [e.g., Buesseler, 1998]. It should be noted that the primary production estimate by Arrigo and van Dijken [2004] was derived from satellite observations and does not account for under-ice algal or subsurface production [e.g., Tremblay *et al.*, 2008; Mundy *et al.*, 2009]. Shadwick *et al.* [2011b] applied an inorganic carbon budget technique to derive a NCP of approximately $2.1 \text{ mol C m}^{-2} \text{ yr}^{-1}$ for the Amundsen Gulf region, 40% of which is supplied by under-ice productivity. According to our estimate, most of the NCP is exported out of the surface layer. Two independent, but similar estimates

of the inventories of respired carbon dioxide (CO_2) in the subsurface waters (50–300 m) of the Amundsen Gulf were recently reported [Shadwick *et al.*, 2011a, 2011b]: $3.8 \text{ mol C m}^{-2} \text{ yr}^{-1}$ and 4.1 mol C m^{-2} . The former was derived by assuming an 18-month residence time for subsurface waters [Lanos, 2009], in line with previous estimates [Yamamoto-Kawai *et al.*, 2008; Hansell *et al.*, 2004] in the region. Our estimate of export production ($1.8 \text{ mol C m}^{-2} \text{ yr}^{-1}$) and the respired CO_2 inventory of 4.1 mol C m^{-2} derived by Shadwick *et al.* [2011a] yield a residence time of the subsurface waters in the Amundsen Gulf on the order of two years, if all the exported carbon is respired in the subsurface waters, in agreement with the residence time reported by Lanos [2009].

[27] The timing of the carbon export reconstructed from this study (Figure 10b) is corroborated by Forest *et al.* [2008], who, based on sediment trap data, reported that the maximum POC contribution to the overall particle flux was observed in May and July, coinciding with the under-ice and pelagic algae blooms and their respective contributions to NCP [Horner and Schrader, 1982; Shadwick *et al.*, 2011b; see also Carmack *et al.*, 2004]. It should be noted, however, that the data of Forest *et al.* [2008] were collected in 2003/2004 and were acquired at a slightly different location. The latter may be of some importance since Forest *et al.* [2008] sampled west of our study area (Figures 1 and 5), likely under a stronger influence of the Mackenzie River plume. Our estimate of export production also depends on the choice of the $\text{C}_{\text{org}}:\text{bio-Ba}$ flux ratio. The ratio we used in this study [$\text{C}_{\text{org}}:\text{bio-Ba} = 225 \text{ g C (g Ba)}^{-1}$ or $2575 \text{ mol C (mol Ba)}^{-1}$] was derived from global or basin-wide estimates in various ocean basins. As noted by Dymond *et al.* [1992], their $\text{C}_{\text{org}}:\text{bio-Ba}$ flux ratio ($185\text{--}200 \text{ g C (g Ba)}^{-1}$) agrees to within 15% of the global estimate reported by Broecker and Peng [1982] ($260 \text{ g C (g Ba)}^{-1}$). On the other hand, as argued by Dehairs *et al.* [2000] and Sternberg *et al.* [2007], the $\text{C}_{\text{org}}:\text{bio-Ba}$ flux ratio may be higher along continental margins, but this has not yet been confirmed for the Arctic shelves. Irrespective of this, higher $\text{C}_{\text{org}}:\text{bio-Ba}$ flux ratios have been attributed to higher carbon fluxes from coastal or margin sites, which in turn would allow our method to assess the export of marine carbon only. This would help constrain results of sediment trap studies, such as those of Forest *et al.* [2008, 2011] or Magen *et al.* [2010] by providing information about the source of the organic matter in the traps. A larger $\text{C}_{\text{org}}:\text{bio-Ba}$ flux ratio would yield higher estimates of our carbon export and would exceed the NCP estimated by Shadwick *et al.* [2011b]. Furthermore, our estimate depends on the riverine Ba concentrations, such that an increase of the riverine Ba concentration by 33% (393 nM Ba instead of 295 nM Ba, Table 1) would increase the carbon export estimate by 24%. Despite the overall uncertainties of our approach, our estimated carbon export of $1.8 \text{ mol C m}^{-2} \text{ yr}^{-1}$, derived from a complete annual data set, serves to better constrain carbon fluxes and production estimates. In addition, since bio-Ba formation and, thus, the Ba fluxes out of the surface layer are closely linked to biological processes in the marine water column, our approach can help unravel the sources of settling organic particles, may they be marine or terrestrial, inorganic or organic [e.g., Forest *et al.*, 2008; Magen *et al.*, 2010].

3.5. The Role of Export Production in the Carbon Budget of Amundsen Gulf

[28] In order to better understand the carbon dynamics of our study area, we establish a carbon budget over the annual cycle using our data and information available from the literature. We considered processes (Figure 11) and assumptions detailed in this section. We derived the CO_2 air-sea exchange from Shadwick *et al.* [2011b], assuming that sea-ice is impermeable to CO_2 , but acknowledge that the latter is currently a focus of ongoing research [e.g., Semiletov *et al.*, 2004; Zemmelink *et al.*, 2006; Papakyriakou and Miller, 2011; Miller *et al.*, 2011; Else *et al.*, 2011; N.-X. Geilfus *et al.*, p CO_2 dynamics and related air-ice CO_2 fluxes in the Arctic coastal zone (Amundsen Gulf, Beaufort Sea, Canada), submitted to *Journal of Geophysical Research*, 2011]. We considered the diffusion of DIC from the subsurface layer into the surface layer (upper 50 m) according to Shadwick *et al.* [2011b]. Since under-ice [Horner and Schrader, 1982; Juul-Pedersen *et al.*, 2010] and subsurface [Tremblay *et al.*, 2008] production plays a crucial role in Arctic Ocean productivity but cannot be captured by satellite imagery, we rely on the primary production estimate by Forest *et al.* [2011], employing a food web model for the period of our observations. We assume that this primary production estimate, obtained for the period March–August 2008, is representative of the overall annual production. We derived NCP from Shadwick *et al.* [2011b], who balanced the inorganic carbon budget in the water column of the Amundsen Gulf. Export production was assessed in this work and we assume that the export of particulate Ba mirrors the export of marine organic matter. Hence, given the export of marine carbon of $0.45 \text{ mol C m}^{-2} \text{ yr}^{-1}$ (see below) out of the subsurface layer (50–100 m), $1.35 \text{ mol C m}^{-2} \text{ yr}^{-1}$ of the $1.8 \text{ mol C m}^{-2} \text{ yr}^{-1}$ exported from the surface layer is respired in the subsurface layer. We considered two estimates for the respiration of organic matter in the subsurface water column: (a) derived from an inorganic carbon budget ($3.8 \text{ mol C m}^{-2} \text{ yr}^{-1}$ [Shadwick *et al.*, 2011b]), and (b) using an estimate of the water column inventory of respired DIC according to Shadwick *et al.* [2011a]. The latter approach was applied to our investigation area, yielding an inventory of 4.1 mol C m^{-2} . Given an 18-month residence time for water below the surface layer, as estimated from a set of hydrographic moorings in the Amundsen Gulf in 2003–2004 [Lanos, 2009], this corresponds to an annual production of $2.7 \text{ mol C m}^{-2} \text{ yr}^{-1}$ for respiratory DIC. The particulate marine and terrestrial organic carbon flux out of the subsurface layer was estimated according to Forest *et al.* [2008, Figure 8b]. This flux estimate, although from a slightly different area, covers almost a full year of observations, compared to that of Forest *et al.* [2011], which cover the period February to July. The extended temporal coverage by Forest *et al.* [2008] is of particular relevance, since our study, and Forest *et al.* [2008], reveal maximum C-export values during summer and autumn (Figure 10), a period not covered by Forest *et al.* [2011]. The benthic respiration was estimated from the particle and sediment biogeochemical study of Renaud *et al.* [2007] using their average sediment oxygen demand of $5 \text{ mmol O}_2 \text{ m}^{-2} \text{ d}^{-1}$. When an O_2 consumption to metabolic CO_2 production ratio of 1.3 [Millero, 2006] is applied for either 6 or 12 months, benthic respiration yields a DIC release

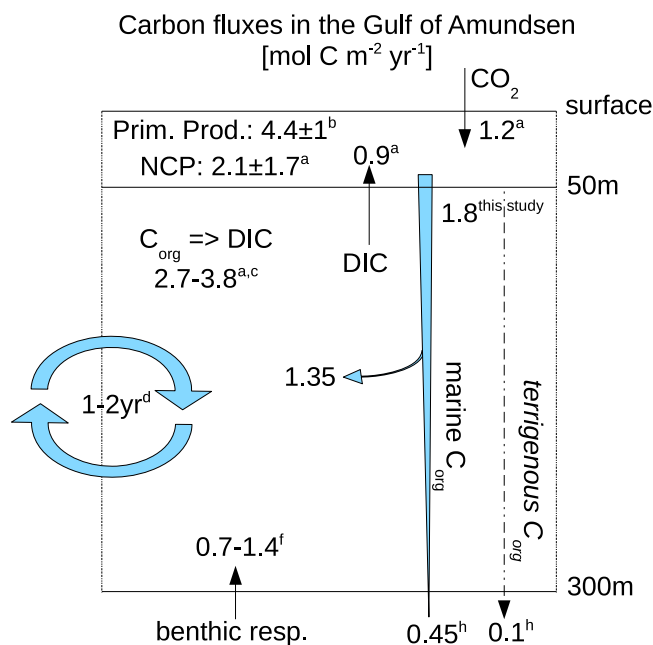


Figure 11. Carbon budget for Amundsen Gulf. Literature values and results of this work are used to estimate the carbon budget for the Amundsen Gulf. Since data were compiled from different years, the budget is climatological rather than for a specific year. Details of the individual terms are given in the text. Sources and times of observations denoted by superscript letters as follows: a, *Shadwick et al.* [2011b], 2007–2008; b, *Forest et al.* [2011], 2008; c, *Shadwick et al.* [2011a], 2007; d, *Lanos* [2009], 2002–2004; f, *Renaud et al.* [2007], 2004; h, *Forest et al.* [2008], 2003–2004.

853 from the surface sediments to the overlying water column
854 of $0.7\text{--}1.4\text{ mol C m}^{-2}\text{ yr}^{-1}$. We assume that there is no
855 net sediment accumulation, i.e., no net carbon burial occurs
856 over annual time-scales in the investigation area [*Richerol*
857 *et al.*, 2008].

858 [29] Despite the considerable uncertainties inherent to all
859 estimated fluxes, the budget presented here can be consid-
860 ered as balanced. The ratio between primary production and
861 NCP or export production [*Arrigo and van Dijken*, 2004;
862 *Forest et al.*, 2011; *Shadwick et al.*, 2011b], respectively, all
863 of which are derived from independent assessments, is on
864 the order of 0.15–0.4. The similarity between the NCP and
865 export fraction supports the hypothesis and observation that,
866 at the annual scale, organic matter does not accumulate in
867 the surface waters. The slightly elevated primary production
868 to export production ratio can be justified by the fact that the
869 under-ice production, which contributes approximately 50%
870 of NCP [*Shadwick et al.*, 2011b], is dominated by diatoms
871 with heavy frustules that sink rapidly [*Horner and Schrader*,
872 1982; *Juul-Pedersen et al.*, 2010]. Furthermore, the spring
873 open water bloom coincides with the peak in river runoff
874 (Figure 10b), which delivers a significant amount of ballast
875 material from land and, in turn, promotes the sinking of
876 marine organic matter, as observed in sediment trap studies
877 [e.g., *Forest et al.*, 2008]. As a result of the respiration of
878 pelagic and benthic, terrigenous and marine organic matter,
879 the DIC in subsurface waters increases by $2.7\text{--}3.8\text{ mol C}$
880 $\text{m}^{-2}\text{ yr}^{-1}$ [*Renaud et al.*, 2007; *Richerol et al.*, 2008]. The

magnitude of benthic respiration is similar to the export rate
of terrigenous and marine organic matter from the subsur-
face layer. On the other hand, it should be stated that, given
the uncertainties of the budget terms, including the residence
time of the subsurface waters, we are presently unable to
determine if lateral inputs of either organic matter or
respired DIC to the study area are significant. It should also
be noted that, since we compiled data from different years,
our proposed budget reflects a climatological view rather
than a budget for any specific year.

4. Conclusions

[30] Dissolved Ba concentrations in the surface waters of
the Canadian Arctic Archipelago display only a slight sea-
sonality because the riverine inputs and the pulse in bio-
logical activity, which is accompanied by bio-Ba formation
and export, occur nearly simultaneously. Formation and
decay of bio-Ba shape the vertical nutrient-type profile of
dissolved Ba in our study area, but the contribution of
authigenic barite dissolution to the water column dissolved
Ba concentrations cannot be distinguished. We exploited
the seasonal Ba deficiency in the surface waters of the
Amundsen Gulf to estimate the particulate organic carbon
export out of the surface layer. This estimate, on the order
of $1.8 \pm 0.45\text{ mol C m}^{-2}\text{ yr}^{-1}$, allowed us to construct a
balanced carbon budget for the Amundsen Gulf. Within this
budget we identified and quantified relevant processes,
including the export of particulate organic carbon and its
subsequent respiration. Nevertheless, the role of lateral
carbon transport into and out of our study area remains to
be evaluated.

[31] **Acknowledgments.** We express our sincere gratitude to the
captains and crews who supported our work during the overwintering of
the CCGS Amundsen. We are grateful to those who helped us sample
for Barium and inorganic carbon parameters. This work is a contribution
to the Canadian IPY programs CFL and GEOTRACES, Swedish Research
Council, the Royal Society of Arts and Sciences, Swedish Research Council
project 2004–4034, to ArcticNet, as well as to the IGBP/IHDP core project
LOICZ. H. Thomas holds a Canada Research Chair. The manuscript greatly
benefited from the comments of two anonymous referees.

References

- Aristegui, J., S. Agustí, J. J. Middelburg, and C. M. Duarte (2005), Respi-
ration in the mesopelagic and bathypelagic zones of the oceans, in
Respiration in Aquatic Ecosystems, edited by P. A. del Giorgio and
P. J. le B. Williams, pp. 181–205, Oxford Univ. Press, New York.
Armstrong, R. A., M. L. Peterson, C. Lee, and S. G. Wakeham (2009),
Settling velocity spectra and the ballast ratio hypothesis, *Deep Sea*
Res., Part II, 56, 1470–1478, doi:10.1016/j.dsr2.2008.11.032.
Arrigo, K. R., and G. L. van Dijken (2004), Annual cycles of sea ice and
phytoplankton in Cape Bathurst polynya, southeastern Beaufort Sea,
Canadian Arctic, *Geophys. Res. Lett.*, 31, L08304, doi:10.1029/
2003GL018978.
Bates, N. R., J. T. Mathis, and L. W. Cooper (2009), Ocean acidification
and biologically induced seasonality of carbonate mineral saturation
states in the Western Arctic Ocean, *J. Geophys. Res.*, 114, C11007,
doi:10.1029/2008JC004862.
Bishop, J. B. K. (1988), The barite-opal-organic carbon association in
oceanic particulate matter, *Nature*, 332, 341–343, doi:10.1038/332341a0.
Broecker, W. S., and T.-H. Peng (1982), *Tracers in the Sea*, 690 pp.,
Lamont-Doherty Geol. Obs., Palisades, N. Y.
Buesseler, K. O. (1998), The de-coupling of production and particulate
export in the surface ocean, *Global Biogeochem. Cycles*, 12, 297–310,
doi:10.1029/97GB03366.
Calvert, S. E., and T. F. Pederson (2007), Elemental proxies for palaeo-
climatic and palaeoceanographic variability in marine sediments:

- 945 Interpretation and application, in *Proxies in the Late Cenozoic Paleoceanography*, edited by C. Hillaire-Marcel and A. de Vernal, pp. 567–644, Elsevier, Amsterdam, doi:10.1016/S1572-5480(07)01019-6.
- 946 Carmack, E. C., R. W. Macdonald, and S. Jasper (2004), Phytoplankton productivity on the Canadian Shelf of the Beaufort Sea, *Mar. Ecol. Prog. Ser.*, 277, 37–50, doi:10.3354/meps277037.
- 947 Chierici, M., A. Fransson, B. Lansard, L. A. Miller, A. Mucci, E. Shadwick, H. Thomas, J.-E. Tremblay, and T. N. Papakyriakou (2011), The impact of biogeochemical processes and environmental factors on the calcium carbonate saturation state in the Circumpolar Flaw Lead in the Amundsen Gulf, Arctic Ocean, *J. Geophys. Res.*, doi:10.1029/2011JC007184, in press.
- 950 Cooper, L. W., J. W. McClelland, R. M. Holmes, P. A. Raymond, J. J. Gibson, C. K. Guay, and B. J. Peterson (2008), Flow-weighted values of runoff tracers ($\delta^{18}\text{O}$, DOC, Ba, alkalinity) from the six largest Arctic rivers, *Geophys. Res. Lett.*, 35, L18606, doi:10.1029/2008GL035007.
- 951 Dehairs, F., W. Baeyens, and L. Goeyens (1992), Accumulation of suspended barite at mesopelagic depths and export production in the Southern Ocean, *Science*, 258, 1332–1335, doi:10.1126/science.258.5086.1332.
- 952 Dehairs, F., D. Shopova, S. Ober, C. Veth, and L. Goeyens (1997), Particulate barium stocks and oxygen consumption in the Southern Ocean mesopelagic water column during spring and early summer: Relationship with export production, *Deep Sea Res., Part II*, 44, 497–516, doi:10.1016/S0967-0645(96)00072-0.
- 953 Dehairs, F., N. Fagel, A. N. Antia, R. Peinert, M. Elskens, and L. Goeyens (2000), Export production in the Bay of Biscay as estimated from barium-barite in settling material: A comparison with new production, *Deep Sea Res., Part I*, 47, 583–601, doi:10.1016/S0967-0637(99)00072-2.
- 954 Dehairs, F., S. Jacquet, N. Savoye, B. A. S. van Mooy, K. O. Buesseler, J. K. B. Bishop, and C. H. Lamborg (2008), Barium in twilight zone suspended matter as a potential proxy for particulate organic carbon remineralization: Results for the North Pacific, *Deep Sea Res., Part II*, 55, 1673–1683, doi:10.1016/j.dsr2.2008.04.020.
- 955 Dickson, A. G., C. L. Sabine, and J. R. Christian (Eds.) (2007), *Guide to Best Practices for Ocean CO₂ Measurements*, PICES Spec. Publ., vol. 3, 191 pp., North Pac. Mar. Sci. Org., Sidney, B. C., Canada.
- 956 Dymond, J., and R. Collier (1996), Particulate barium fluxes and their relationships to biological productivity, *Deep Sea Res., Part II*, 43, 1283–1308, doi:10.1016/0967-0645(96)00011-2.
- 957 Dymond, J., E. Suess, and M. Lyle (1992), Barium in deep-sea sediment: A geochemical proxy for paleoproductivity, *Paleoceanography*, 7, 163–181, doi:10.1029/92PA00181.
- 958 Else, B. G. T., T. N. Papakyriakou, R. J. Galley, W. M. Drennan, L. A. Miller, and H. Thomas (2011), Wintertime CO₂ fluxes in an Arctic polynya using eddy covariance: Evidence for enhanced air-sea gas transfer during ice formation, *J. Geophys. Res.*, 116, C00G03, doi:10.1029/2010JC006760.
- 959 Falkner, K. K., R. W. Macdonald, E. C. Carmack, and T. Weingartner (1994), The potential of barium as tracer of Arctic water masses, in *The Polar Oceans and Their Role in Shaping the Global Environment*, *Geophys. Monogr. Ser.*, vol. 85, edited by O. M. Johannessen, R. D. Muench, and J. E. Overland, pp. 63–76, AGU, Washington, D. C.
- 960 Forest, A., M. Sampei, R. Makabe, H. Sasaki, D. G. Barber, Y. Gratton, P. Wassmann, and L. Fortier (2008), The annual cycle of particulate organic carbon export in Franklin Bay (Canadian Arctic): Environmental control and food web implications, *J. Geophys. Res.*, 113, C03S05, doi:10.1029/2007JC004262.
- 961 Forest, A., et al. (2011), Biogenic carbon flows through the planktonic food web of the Amundsen Gulf (Arctic Ocean): A synthesis of field measurements and inverse modeling analyses, *Prog. Oceanogr.*, doi:10.1016/j.pocean.2011.05.002, in press.
- 962 Francois, R., S. Honjo, S. J. Manganini, and G. E. Ravizza (1995), Biogenic barium fluxes to the deep sea: Implications for paleoproductivity reconstruction, *Global Biogeochem. Cycles*, 9, 289–303, doi:10.1029/95GB00021.
- 963 Gillikin, D. P., F. Dehairs, A. Lorrain, D. Steenmans, W. Baeyens, and L. André (2006), Barium uptake into shells of the common mussel (*Mytilus edulis*) and the potential for estuarine paleo-chemistry reconstruction, *Geochim. Cosmochim. Acta*, 70, 395–407, doi:10.1016/j.gca.2005.09.015.
- 964 Guay, C. K., and K. K. Falkner (1997), Barium as tracer of Arctic halocline and river waters, *Deep Sea Res., Part II*, 44, 1543–1569, doi:10.1016/S0967-0645(97)00066-0.
- 965 Guay, C. K., and K. K. Falkner (1998), A survey of dissolved barium in the estuaries of the major Arctic rivers and adjacent seas, *Cont. Shelf Res.*, 18, 859–882, doi:10.1016/S0278-4343(98)00023-5.
- 966 Guay, C. K. H., F. A. McLaughlin, and M. Yamamoto-Kawai (2009), Differentiating fluvial components of upper Canada Basin waters on the basis of measurements of dissolved barium combined with other physical and chemical tracers, *J. Geophys. Res.*, 114, C00A09, doi:10.1029/2008JC005099.
- 967 Hansell, D. A., D. Kadko, and N. R. Bates (2004), Degradation of terrigenous dissolved organic carbon in the western Arctic Ocean, *Science*, 304, 858–861, doi:10.1126/science.1096175.
- 968 Hoppema, M., F. Dehairs, J. Navez, C. Monnin, C. Jeandel, E. Fahrback, and H. J. W. de Baar (2010), Dissolved barium distributions in the Weddell Gyre: Impact of circulation and biogeochemical processes, *Mar. Chem.*, 122, 118–129, doi:10.1016/j.marchem.2010.07.005.
- 969 Horner, R., and G. C. Schrader (1982), Relative contributions of ice algae, phytoplankton and benthic microalgae to primary production in near-shore regions of the Beaufort Sea, *Arctic*, 35, 485–503.
- 970 Jacquet, S. H. M. (2007), Barium in the Southern Ocean: Towards an estimation of twilight zone C mineralization, Ph.D. dissertation, 234 pp., Vrije Univ. Brussel, Brussels.
- 971 Jacquet, S. H. M., F. Dehairs, D. Cardinal, J. Navez, and B. Dellile (2005), Barium distribution across the Southern Ocean frontal system in the Crozet-Kerguelen Basin, *Mar. Chem.*, 95, 149–162, doi:10.1016/j.marchem.2004.09.002.
- 972 Jacquet, S. H. M., F. Dehairs, M. Elskens, N. Savoye, and D. Cardinal (2007), Barium cycling along WOCE SR3 line in the Southern Ocean, *Mar. Chem.*, 106, 33–45, doi:10.1016/j.marchem.2006.06.007.
- 973 Juul-Pedersen, T., C. Michel, and M. Gosselin (2010), Sinking export of particulate organic material from the euphotic zone in the eastern Beaufort Sea, *Mar. Ecol. Prog. Ser.*, 410, 55–70, doi:10.3354/meps08608.
- 974 Kellogg, C. T. E., S. D. Carpenter, A. A. Renfro, A. Sallon, C. Michel, J. K. Cochran, and J. W. Deming (2011), Evidence for microbial attenuation of particle flux in the Amundsen Gulf and Beaufort Sea: Elevated hydrolytic enzyme activity on sinking aggregates, *Polar Biol.*, doi:10.1007/s00300-011-1015-0, in press.
- 975 Lanos, R. (2009), Circulation régionale, masses d'eau, cycles d'évolution et transports entre la mer de Beaufort et le golfe d'Amundsen, Ph.D. thesis, Univ. du Québec, Québec, Canada.
- 976 Lavoie, D., R. W. Macdonald, and K. L. Denman (2009), Primary productivity and export fluxes on the Canadian shelf of the Beaufort Sea: A modelling study, *J. Mar. Syst.*, 75, 17–32, doi:10.1016/j.jmarsys.2008.07.007.
- 977 Macdonald, R. W., E. C. Carmack, F. McLaughlin, K. Iseki, D. Macdonald, and M. O'Brien (1989), Composition and modification of water masses in the Mackenzie shelf estuary, *J. Geophys. Res.*, 94, 18,057–18,070, doi:10.1029/JC094iC12p18057.
- 978 Magen, C., G. Chaillou, S. A. Crowe, A. Mucci, B. Sundy, A. Gao, R. Makabe, and H. Sasaki (2010), Origin and fate of particulate organic matter in the Southern Beaufort Sea—Amundsen Gulf region, Canadian Arctic, *Estuarine Coastal Shelf Sci.*, 86, 31–41, doi:10.1016/j.ecss.2009.09.009.
- 979 Miller, L. A., T. N. Papakyriakou, R. E. Collins, J. W. Deming, J. K. Ehn, R. W. Macdonald, A. Mucci, O. Owens, M. Raudsepp, and N. Sutherland (2011), Carbon dynamics in sea ice: A winter flux time series, *J. Geophys. Res.*, 116, C02028, doi:10.1029/2009JC006058.
- 980 Millero, F. J. (2006), *Chemical Oceanography*, 3rd ed., 531 pp., CRC Press, Boca Raton, Fla.
- 981 Monnin, C. (1999), A thermodynamic model for the solubility of barite and celestine in electrolyte solutions and seawater to 200°C and 1 kbar, *Chem. Geol.*, 153(1–4), 187–209, doi:10.1016/S0009-2541(98)00171-5.
- 982 Monnin, C., C. Jeandel, T. Cattaldo, and F. Dehairs (1999), The marine barite saturation state of the world's ocean, *Mar. Chem.*, 65, 253–261, doi:10.1016/S0304-4203(99)00016-X.
- 983 Mucci, A., B. Lansard, L. A. Miller, and T. N. Papakyriakou (2010), CO₂ fluxes across the air-sea interface in the southeastern Beaufort Sea: The ice-free period, *J. Geophys. Res.*, 115, C04003, doi:10.1029/2009JC005330.
- 984 Münchow, A., and H. Melling (2008), Ocean current observations from Nares Strait to the west of Greenland: Interannual to tidal variability and forcing, *J. Mar. Res.*, 66, 801–833.
- 985 Mundy, C. J., et al. (2009), Contribution of under-ice primary production to an ice-edge upwelling phytoplankton bloom in the Canadian Beaufort Sea, *Geophys. Res. Lett.*, 36, L17601, doi:10.1029/2009GL038837.
- 986 Papakyriakou, T., and L. A. Miller (2011), Springtime CO₂ exchange over seasonal sea ice in the Canadian Arctic Archipelago, *Ann. Glaciol.*, 52(57), 215–224, doi:10.3189/172756411795931534.
- 987 Prange, M. (2002), Einfluss arktischer Süßwasserquellen auf die Zirkulation im Nordmeer und im Nordatlantik in einem prognostischen Ozean-Meereis-Modell, Ph.D. thesis, Univ. of Bremen, Bremen, Germany.
- 988 Renaud, P. E., A. Riedel, C. Michel, N. Morata, M. Gosselin, T. Juul-Pedersen, and A. Chiuchio (2007), Seasonal variation in benthic community oxygen demand: A response to an ice algal bloom in the Beaufort Sea, Canadian Arctic?, *J. Mar. Syst.*, 67, 1–12, doi:10.1016/j.jmarsys.2006.07.006.

- 1102 Richerol, T., A. Rochon, S. Blasco, D. B. Scott, T. M. Schell, and R. J. 1145
 1103 Bennett (2008), Distribution of dinoflagellate cysts in surface sediments 1146
 1104 of the Mackenzie Shelf and Amundsen Gulf, Beaufort Sea (Canada), 1147
 1105 *J. Mar. Syst.*, **74**, 825–839, doi:10.1016/j.jmarsys.2007.11.003. 1148
 1106 Semiletov, I., A. Makshtas, S.-I. Akasofu, and E. Andreas (2004), Atmo- 1149
 1107 spheric CO₂ balance: The role of Arctic sea ice, *Geophys. Res. Lett.*, 1150
 1108 **31**, L05121, doi:10.1029/2003GL017996. 1151
 1109 Shadwick, E. H., H. Thomas, Y. Gratton, D. Leong, S. Moore, T. N. 1152
 1110 Papakyriakou, and A. E. F. Prowe (2011a), Export of Pacific carbon 1153
 1111 through the Arctic Archipelago to the North Atlantic, *Cont. Shelf Res.*, 1154
 1112 **31**, 806–816, doi:10.1016/j.csr.2011.01.014. 1155
 1113 Shadwick, E. H., et al. (2011b), Seasonal variability of the inorganic carbon 1156
 1114 system in the Amundsen Gulf region of the southeastern Beaufort Sea, 1157
 1115 *Limnol. Oceanogr.*, **56**, 303–322, doi:10.4319/lo.2011.56.1.0303. 1158
 1116 Sternberg, E., D. Tang, T.-Y. Ho, C. Jeandel, and F. M. M. Morel (2005), 1159
 1117 Barium uptake and adsorption in diatoms, *Geochim. Cosmochim. Acta*, 1160
 1118 **69**, 2745–2752, doi:10.1016/j.gca.2004.11.026. 1161
 1119 Sternberg, E., C. Jeandel, J.-C. Miquel, B. Gasser, M. Souhaut, R. Arraes- 1162
 1120 Mescoff, and R. Francois (2007), Particulate barium fluxes and export 1163
 1121 production in the northwestern Mediterranean, *Mar. Chem.*, **105**, 281–295, 1164
 1122 doi:10.1016/j.marchem.2007.03.003. 1165
 1123 Sternberg, E., C. Jeandel, E. Robin, and M. Souhaut (2008), Seasonal cycle 1166
 1124 of suspended barite in the mediterranean sea, *Geochim. Cosmochim. 1167*
 1125 *Acta*, **72**, 4020–4034, doi:10.1016/j.gca.2008.05.043. 1168
 1126 Taylor, J. R., K. K. Falkner, U. Schauer, and M. Meredith (2003), Quanti- 1169
 1127 tative considerations of dissolved barium as a tracer in the Arctic Ocean, 1170
 1128 *J. Geophys. Res.*, **108**(C12), 3374, doi:10.1029/2002JC001635. 1171
 1129 Tremblay, J., K. Simpson, J. Martin, L. Miller, Y. Gratton, D. Barber, 1172
 1130 and N. M. Price (2008), Vertical stability and the annual dynamics of 1173
 1131 nutrients and chlorophyll fluorescence in the coastal, southeast Beaufort 1174
 1132 Sea, *J. Geophys. Res.*, **113**, C07S90, doi:10.1029/2007JC004547. 1175
 1133 van Beek, P., E. Sternberg, J.-L. Reyss, M. Souhaut, E. Robin, and C. Jeandel 1176
 1134 (2009), ²²⁸Ra/²²⁶Ra and ²²⁶Ra/Ba ratios in the Western Mediterranean Sea: 1177
 1135 Barite formation and transport in the water column, *Geochim. Cosmochim. 1178*
 1136 *Acta*, **73**, 4720–4737, doi:10.1016/j.gca.2009.05.063. 1179
 1137 Yamamoto-Kawai, M., and N. Tanaka (2005), Freshwater and brine beha- 1180
 1138 viors in the Arctic Ocean deduced from historical data of $\delta^{18}\text{O}$ and alka- 1181
 1139 linity (1992–2002 A.D.), *J. Geophys. Res.*, **110**, C10003, doi:10.1029/ 1182
 1140 2004JC002793. 1183
 1141 Yamamoto-Kawai, M., F. A. McLaughlin, E. C. Carmack, S. Nishino, and 1184
 1142 K. Shimada (2008), Freshwater budget of the Canada basin, Arctic Ocean, 1185
 1143 from salinity, $\delta^{18}\text{O}$ and nutrients, *J. Geophys. Res.*, **113**, C01007, 1186
 1144 doi:10.1029/2006JC003858. 1187
- M. Chierici, Department of Chemistry, University of Gothenburg, 1157
 Kemiv. 10, SE-41296 Göteborg, Sweden. 1158
 F. Dehairs and J. Navez, Earth System Sciences and Analytical and 1159
 Environmental Chemistry, Vrije Universiteit Brussel, Pleinlaan 2, B-1050 1160
 Brussels, Belgium. 1161
 A. Fransson, Department of Earth Sciences, University of Gothenburg, 1162
 PO Box 460, SE-40530 Göteborg, Sweden. 1163
 Y. Gratton, INRS-ETE, 490 de la Couronne, Quebec, QC G1K 9A9, 1164
 Canada. 1165
 B. Lansard and A. Mucci, Department of Earth and Planetary Sciences, 1166
 McGill University, 3450 University St., Montreal, QC H2A 3A7, Canada. 1167
 L. A. Miller, Institute of Ocean Sciences, Fisheries and Oceans Canada, 1168
 PO Box 6000, Sidney, BC V8L 4B2, Canada. 1169
 C. Monnin, Laboratoire Mécanismes et Transferts en Géologie, CNRS- 1170
 Université Paul Sabatier, F-31400 Toulouse, France. 1171
 T. N. Papakyriakou, Center for Earth Observation Science, University of 1172
 Manitoba, 470 Wallace Bldg., 125 Dysart Rd., Winnipeg, MB R3T 2N2, 1173
 Canada. 1174
 F. Prowe, Leibniz Institute of Marine Sciences at University of Kiel 1175
 (IFM-GEOMAR), Duesternbrooker Weg 20, D-24105, Kiel, Germany. 1176
 E. Shadwick, Antarctic Climate and Ecosystems Cooperative Research 1177
 Center, Hobart, TAS, Australia. 1178
 H. Thomas and E. Sternberg, Department of Oceanography, Dalhousie 1179
 University, 1355 Oxford St., Halifax, NS B3H 4J1, Canada. (helmuth. 1180
 thomas@dal.ca) 1181
 J.-É. Tremblay, Department de Biologie, Université Laval, Pavillon 1182
 Alexandre-Vachon, Quebec, QC G1V 0A6, Canada. 1183